INVESTIGATION OF PUNCHING SHEAR DESIGN APPROACHES IN TURKISH BUILDING EARTHQUAKE SPECIFICATION FOR INTERIOR SLAB-COLUMN CONNECTIONS

A THESIS SUBMITTED TO
THE GRADUATE SCHOOL OF NATURAL AND APPLIED SCIENCES
OF
MIDDLE EAST TECHNICAL UNIVERSITY

BY

MUSTAFA YAVUZ ÖZDEN

IN PARTIAL FULFILLMENT OF THE REQUIREMENTS
FOR
THE DEGREE OF MASTER OF SCIENCE
IN
CIVIL ENGINEERING

JANUARY 2023

Approval of the thesis:

INVESTIGATION OF PUNCHING SHEAR DESIGN APPROACHES IN TURKISH BULDING EARTHQUAKE SPECIFICATION FOR INTERIOR SLAB-COLUMN CONNECTIONS

submitted by **MUSTAFA YAVUZ ÖZDEN** in partial fulfillment of the requirements for the degree of **Master of Science** i**n Civil Engineering, Middle East Technical University** by,

Prof. Dr. Halil Kalıpçılar
Dean, Graduate School of **Natural and Applied Sciences** _____

Prof. Dr. Erdem Canbay
Head of the Department, **Civil Engineering** _____

Prof. Dr. Barış Binici
Supervisor, **Civil Engineering, METU** _____

Examining Committee Members:

Prof. Dr. Ahmet Yakut
Civil Engineering, METU _____

Prof. Dr. Barış Binici
Civil Engineering, METU _____

Prof. Dr. Özgür Kurç
Civil Engineering, METU _____

Prof. Dr. Erdem Canbay
Civil Engineering, METU _____

Assist. Prof. Dr. Hakan Erdoğan
Civil Engineering, Kocaeli University _____

Date: 26.01.2023

I hereby declare that all information in this document has been obtained and presented in accordance with academic rules and ethical conduct. I also declare that, as required by these rules and conduct, I have fully cited and referenced all material and results that are not original to this work.

Name Last name : Özden, Mustafa Yavuz

Signature :

ABSTRACT

INVESTIGATION OF PUNCHING SHEAR DESIGN APPROACHES IN TURKISH BUILDING EARTHQUAKE SPECIFICATION FOR INTERIOR SLAB-COLUMN CONNECTIONS

Özden, Mustafa Yavuz
Master of Science, Civil Engineering
Supervisor: Prof. Dr. Barış Binici

January 2023, 87 pages

Flat plate sytems are very critical due to possible punching failure at slab-column connections. Importance of having reliable design and guidelines on punching shear design of slab-column connections under lateral loads have been shown in the past for zones under high seismic risk. In the new Turkish Building Earthquake Specification published at 2018, there are two different method to analyze slab-column connections. First one is eccentric shear stress model which is also included in ACI 318-19. Second one is the use of finite element method. In this study, analysis methods included in the new Turkish Specification, TBDY 2018 for slab-column connections were evaluated in the light of experimental results. Moment capacities of interior slab-column connections of experimental test specimens were estimated by using two different analysis method i.e. eccentric shear stress model and finite element model then results were compared with expereimental results. In the scope of the finite element model, two different approaches were examined to estimate moment capacity of the connection. In addtion, effect of mesh size were also investigated for the finite element analysis based design. Effect of flexural reinforcement ratio and gravity shear ratio on the ratio of unbalanced moment carried

by eccentric shear (γ_v) was also investigated and simple proposal was made. While estimating the new γ_v, only experimental results of square column were used to ignore effects of column aspect ratio on the ratio of unbalanced moment carried by eccentric shear.

Keywords: Flat-Plate Slab Systems, Punching Shear Design, Eccentric Shear Stress Model, Finite element model, Ratio of unbalanced moment carried by eccentric shear (γ_v), Flexural reinforcement ratio (ρ), gravity shear ratio (V_u/V_n)

ÖZ

DÖŞEME İÇ KOLON BİRLEŞİMLERİ İÇİN TÜRKİYE BİNA DEPREM YÖNETMELİĞİNDE BULUNAN ZIMBALAMA TASARIM YAKLAŞIMLARININ İNCELENMESİ

Özden, Mustafa Yavuz
Yüksek Lisans, İnşaat Mühendisliği
Tez Yöneticisi: Prof. Dr. Barış Binici

Ocak 2023, 87 sayfa

Kirişiz döşemeli sistemler döşeme kolon bağlantılarındaki olası zımbalama problemi nedeniyle çok kritik yapılardır. Özellikle sismik riskin yüksek olduğu bölgelerde yatay yüke maruz kalan döşeme kolon bağlantılarının zımbalama açısından güvenilir tasarıma ve yönetmeliklere sahip olmasının önemi geçmişte gösterilmiştir. 2018 yılında yayınlanan yeni Türkiye Bina Deprem Yönetmeliğinde, döşeme-kolon bağlantılarının analizi için iki farklı yöntem bulunmaktadır. Bunlardan birinci, ACI 318-19'da da yer alan eksantrik kayma gerilmesi modelidir. İkinci ise sonlu elemanlar yönteminin kullanılmasıdır. Bu çalışma kapsamında bu iki analiz yöntemi deneysel sonuçlar ışığında değerlendirilmiştir. Bu iki yöntem kullanılarak daha önce yapılan deneylerdeki döşeme-iç kolon bağlantılarının moment kapasiteleri hesaplanmış ve deneyde elde edilen sonuçlar ile karşılaştırılmıştır. Sonlu eleman modeli kapsamında iki farklı yaklaşım incelenmiştir. Ek olarak, kabuk eleman boyutlarının sonlu eleman modeli sonuçlarını nasıl etkilediği de incelenmiştir. Eğilme donatısı oranı ve düşey yükün düşey yük taşıma kapasitesine oranının, γ_v katsayısı üzerindeki etkisi araştırılmış ve γ_v katsayısı tahmini için basit bir öneride

bulunulmuştur. γ_v katsayısı hesaplanırken sadece kare kolona sahip test numunelerinin sonuçları kullanılmış ve kolon en-boy oranı etkisi ihmal edilmiştir.

Anahtar Kelimeler: Kirişsiz Döşemeli Sistemler, Zımbalama Tasarımı, Eksantrik Kayma Gerilmesi Modeli, Sonlu Elemanlar Yöntemi, γ_v Katsayısı, Eğilme Donatısı Oranı, Düşey Yükün Düşey Yük Taşıma Kapasitesine Oranı

To my grandfather and grandmother in heaven

Mustafa Özden and Hasibe Özden

ACKNOWLEDGMENTS

I would like to start my words by thanking my advisor Prof. Dr. Barış Binici for his help, support, and strong guidelines. It was honor to work with him.

I would also like to thank my manager, Dr. Cenan Özkaya who has important role of improvement on my engineering career for his encouragement and technical support to finish my master thesis.

I also thank my friends, Celil Orak and Berk Bora Çakır for their supports to increase my motivation.

I am thankful to Ayşe Asena Sarıçiçek who one of the biggest supporters in my life. I know she always will be with me in every special and hard moment in my life.

I would like to thank my grandfather, Mehmet Bayırlı and my grandmother, Nuriye Bayırlı. I know I am always in their prayers.

I am thankful to my sister, Hilal Özden. I always feel lucky to have her love.

Last and biggest my thanking is for my father, Yaşar Özden and my mother, Hatice Özden. I couldn't come to this day without their supports and encouragement. I am sure they deserve this diploma more than me. I want to dedicate this diploma to them.

TABLE OF CONTENTS

LIST OF TABLES

TABLES

LIST OF FIGURES

FIGURES

CHAPTER 1

INTRODUCTION

1.1 Flat-Plate Systems

Unlike the commonly used structural systems constructed with slabs, beams, and columns, flat-plate systems consist of slabs directly supported on the columns. These systems are very common and preferable because of their advantages listed below.

- Usage of simple formwork and ease of construction
- Reduced construction time compared to the traditional frame systems
- Ease of architectural implementation due to lack of beams

These types of systems are generally used in low and moderate seismic zones because slab-column connections are very flexible and vulnerable to have severe damage when subjected to high lateral force. Behavior of slab-column connections is rather well known when subjected to only vertical loads and structural guidelines were established based on large databases. (CEB/fib Task Group, 2001)

Flat plate systems are also usually used with shear walls to increase lateral resistance and prevent excessive drifts. Combination of gravity shear force and shear force caused by transferred moment due to lateral deformation demand is observed to result in possible catastrophic and brittle punching shear failure. (Binici, B., 2003)

There are some strength enhancement methods like a drop panel, column heads or combination of two to increase the punching shear strength. Some examples are shown in Figures 1.1. Despite these options, use of flat plates is still commonly used due to their construction advantages.

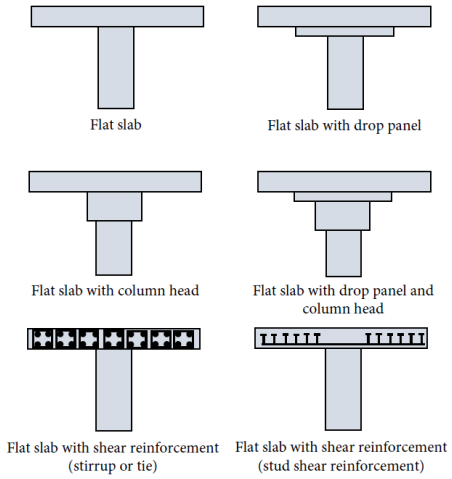

Figure 1.1 Types of Strength Enhancement Methods

Shear reinforcement is another strength enhancement method to increase punching shear capacity. There are different types of shear reinforcement like a stirrup or tie and shear studs in Figure 1.1. Even if shear strength can be increased by using each shear reinforcement type, high ductility is provided by using shear studs with maximum efficiency. Megally and Ghali (2000) investigated effects of shear reinforcements on the slab-column connections. It was shown that stud shear reinforcement increases ductility as well as shear strength. Shear strength versus maximum slab deflection relationship for different strength enhancement methods is shown at Figure 1.2. (Megally and Ghali, 2000)

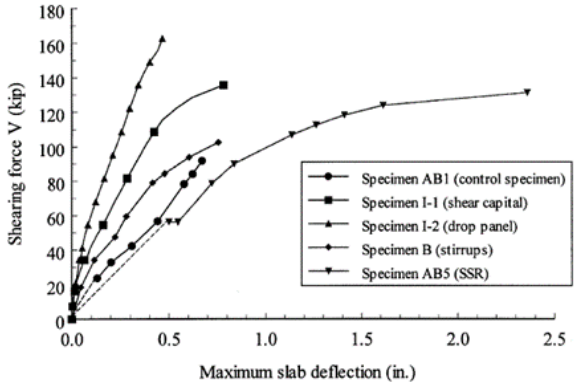

Figure 1.2 Comparison of strength enhancement methods for slab-column connections in terms of shear strength and ductility (Megally and Ghali, 2000)

1.2 Failure Mechanism and Punching Shear Failure Examples

During punching shear failures, due to the excessive shear stress concentration on slab around the column, slab moves down independently and separated from the slab at vicinity of the column. That is the sudden and catastrophic failure mode, which is called punching shear failure illustrated in Figure 1.3.

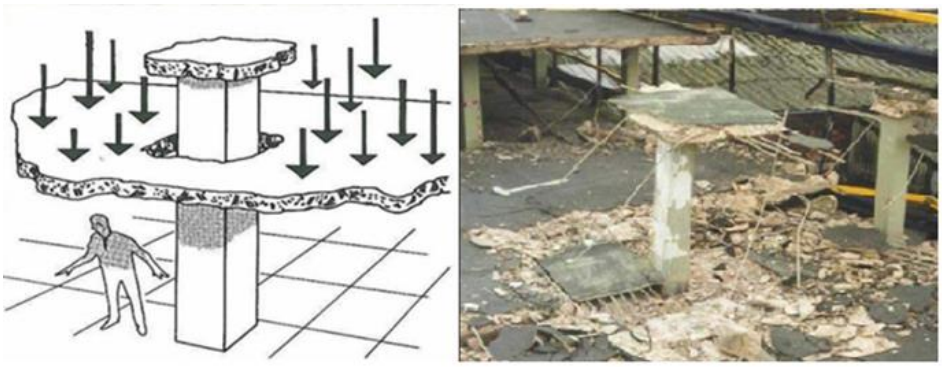

Figure 1.3 Punching Shear Failure (civilengdis.com)

While cracks on top of the slab start at distance d (effective depth of slab) far away from the column face, they start at face of the column on the bottom of the slab. This means that slope of the crack line is equal to approximately 45°. Shear stress at the vicinity of the column consist of two parts which are shear stress caused by gravitational load and shear stress caused by transferred unbalanced moment on the connection. Failure mechanism is also illustrated in Figure 1.4.

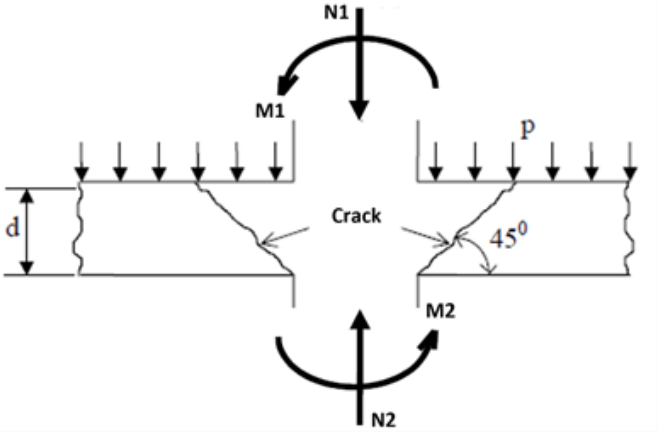

Figure 1.4 Failure Mechanism

Examples of punching shear failure induced collapse can be found in the literature.

Figure 1.5 Bullock's Department Store after Collapse (deseret.com)

Main reason of the failure is shear stress caused by gravitational shear force and unbalanced moment on the slab-column connection because of earthquake occurred in 1994, in California. Although this building was constructed with shear walls, failure was not prevented. (Zorlu, M., 2012) Building view after collapse is shown in Figure 1.5.

Figure 1.6 Waffle Slab Buildings at Mexico City after Earthquake Occurred in 1985 (johnmartin.com)

Many waffle slab buildings collapsed because of the earthquake in 1985 at Mexico City. Main reason of collapse is that lateral drift is not prevented enough for these buildings. (Zorlu, M., 2012) View of some buildings after collapse is shown in Figure 1.6.

1.3 Punching Shear Design Methods in TBDY 2018

In the Turkish Building Earthquake Specification published in 2018, there are two different methods to find critical punching shear stress on the perimeter of slab-column connections. First one is the use of the eccentric shear stress model which is very common and a practical approach, presented in the American Specification, ACI 318-19. It assumes shear stress is distributed linearly at the critical zone located d/2 away from the column face and it gives engineers to have opportunity to calculate amount of contribution of flexural moment and moment cause to shear stress separately depending on column aspect ratio. Apart from column aspect ratio, necessary parameters are the moment and gravitational shear force on the slab-column connection. Second method is calculating critical shear stress on the perimeter of slab-column connections directly from finite element analysis. Specification allows engineers to create whole structure model and find critical shear stress on the perimeter directly from the shell elements according to critical load combinations.

1.3.1 Eccentric Shear Stress Model

In the scope eccentric shear stress model method, unbalanced moment caried by flexure (γ_f) is calculated with Equation 1.1.

$$\gamma_f = \frac{1}{1 + \left(\frac{2}{3}\right)\sqrt{\frac{b_1}{b_2}}} \tag{1.1}$$

In this equation, b_1 is the dimension of perimeter in the lateral loading direction, b_2 is the dimension of perimeter in direction perpendicular to the loading direction. Dimensions of perimeter is specified by summing of dimensions of column and effective depth of the slab by using Equation 1.2 and 1.3. Critical punching shear perimeter is found with Equation 1.4.

$$b_1 = d + c_1 \tag{1.2}$$

$$b_2 = d + c_2 \tag{1.3}$$

$$u_p = 2 \times (d + c_1) + 2 \times (d + c_2) \tag{1.4}$$

Here, d is effective depth of the slab. Effective depth of the slab is distance from top or bottom layer of the slab to the outermost layer of flexural tension reinforcement. In addition, c_1 and c_2 are dimensions of column in two directions. Placement of critical punching perimeter around the column in Figure 1.7.

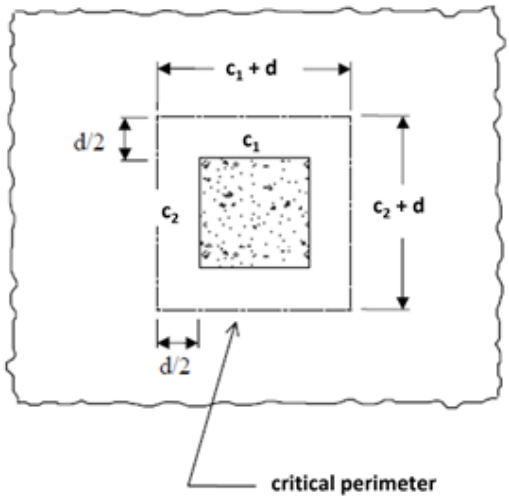

Figure 1.7 Critical Punching Perimeter of Interior Slab-Column Connection

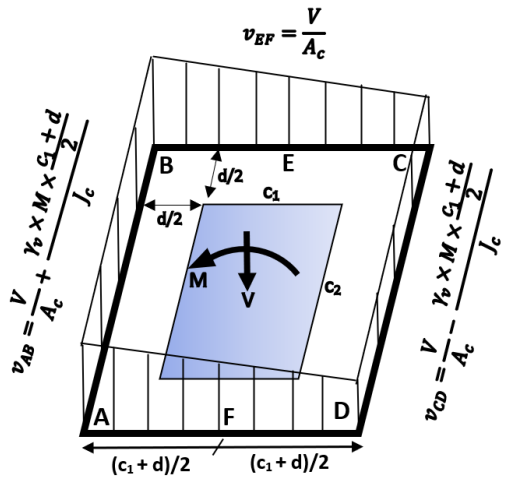

Figure 1.8 Assumed Shear Stress Distribution according to Eccentric Shear Stress Model

Multiplying the connection moment which is equal to sum of moment at top and bottom of slab on the column with γ_f gives amount of flexural moment on the slab. The amount of flexural reinforcement must be at least to carry flexural moment calculated with γ_f value. Remaining part of the moment on the connection which is obtained by multiplying of total moment on the slab-column connection with γ_v must be carried by the shear capacity of the slab. γ_v is calculated with Equation 1.5.

$$\gamma_v = 1 - \gamma_f \tag{1.5}$$

Critical shear stress on the punching perimeter of slab column connections subjected to lateral loads in one direction is calculated with Equation 1.6.

$$v_c = \frac{V_u}{A_c} \pm \frac{\gamma_v \times M_u \times c}{J_c} \tag{1.6}$$

Shear stress caused by gravitational shear force is calculated in the first term of Equation 1.6. Here, V_u is the ultimate shear force caused by the dead load and superimposed dead load on the connection. A_c is the critical area subjected to punching shear force which is found multiplying of perimeter and effective slab depth. Equation 1.7 is used for the calculation of the critical area subjected to punching shear force. M_u is the unbalanced moment on the slab-column connection. It is equal to the sum of column moment M_1 and M_2 which are transferred to the connection. M_1 and M_2 is previously shown in Figure 1.4. Equation 1.8 is used for calculation of M_u. J_c is a parameter similar to the polar moment of inertia of the critical zone, c is the distance between outer layer of perimeter to the midpoint of the perimeter. Formulas of J_c and distance c are given in Equation 1.9 and 1.10 respectively.

$$A_c = u_p \times d \tag{1.7}$$

$$M_u = M_1 + M_2 \tag{1.8}$$

$$J_c = \frac{d \times (c_1 + d)^3}{6} + \frac{(c_1 + d) \times d^3}{6} + \frac{d \times (c_1 + d)^2 \times (c_2 + d)}{2} \tag{1.9}$$

$$c = \frac{b_1 \; or \; b_2}{2} \tag{1.10}$$

Final assumed shear stress distribution on the critical punching perimeter of interior slab-column connection subjected to lateral load in only one direction is shown in Figure 1.8.

1.3.2 Finite Element Model

There are two types of finite element approaches commonly used to model slab on the building. These are rigid diaphragm and semi-rigid diaphragm. Depending on the conditions, both can be used for modelling purposes. If stiffness of the slab is sufficiently high, slab can be modelled with rigid diaphragm considering that it behaves like a rigid member. Lateral resisting members such as beam, column and shear wall are linked with rigid members to each other. Self-weight and additional dead loads are defined at the center of story. It is assumed that slab doesn't deform in its plane for the rigid diaphragm assumption. Therefore, in-plane stresses are not obtained by using this approach. Unlike the rigid diaphragm, semi rigid diaphragm allows to distribute self-weight and dead load to whole story by using shell elements while modelling of the slab. It also gives opportunity to observe in-plane stresses of slab considering changing of shape of slab under bending and axial forces. Because of in-plane effects included in analysis, it gives more accurate and sensitive results.

Semi-rigid diaphragm is used

- to model structures have irregularity on plan
- to model structures have discontinuity on the slab.
- to model flat plate buildings
- to model buildings have ribbed slab

Modelling whole structure by using two different approach is illustrated in Figure 1.9.

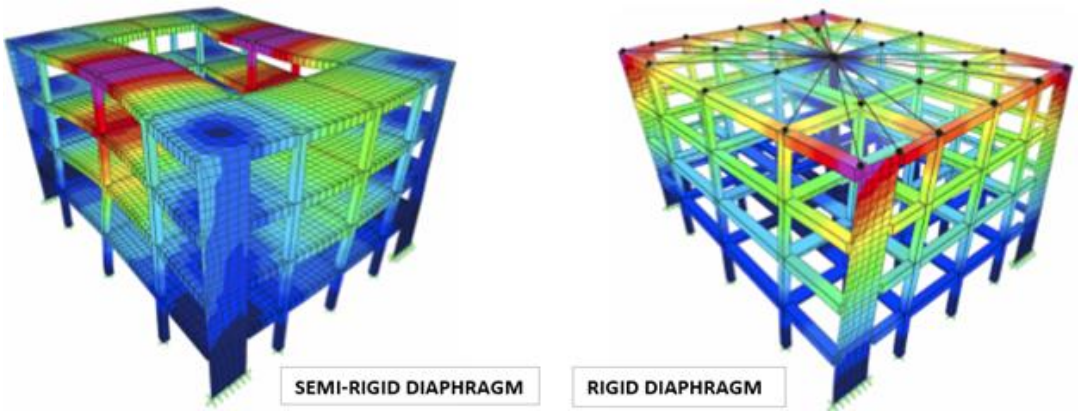

Figure 1.9 Modelling of Whole Structure Using Semi-Rigid and Rigid Diaphragm Approaches (ideCAD.com)

In Turkish Specification, TBDY 2018, semi-rigid diaphragm is recommended for modelling of the flat plate buildings. Using of rigid diaphragm approach is not permitted for modelling of flat plate systems. Additionally, Turkish specification allows directly to use shear stress values which is obtained from shell elements for punching design of slab-column connection. Here, important issue is the fact that shear stresses must be read at a distance d/2 far away from the column face and shear stresses must be lower than shear strength. Equation 1.11 included in TBDY 2018 is given for the design of slab-column connection by using the finite element model. Depending on whether Equation 1.11 is satisfied or not, it is decided if shear reinforcement is needed.

$$T = \frac{V_u}{d} \leq f_{ctd} \tag{1.11}$$

In Equation 1.11, T is shear stress, V_u is shear forces per unit width from shell elements, d is the effective depth of slab and f_{ctd} is tensile strength of concrete. It is obvious that V_u shows variations from node to node within critical zone mesh.

1.4 Punching Design Approach in Eurocode 2

Eccentric shear stress model in TBDY 2018 is presented in Section 1.3.1. This model is also included in ACI 318. Different version of eccentric shear stress model included in Eurocode 2 is presented in this section.

Critical punching perimeter for rectangular column is shown at Figure 1.10. Necessary formula to calculate punching perimeter is shown in Equation 1.12.

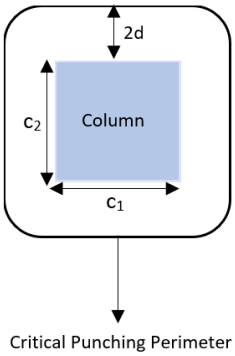

Figure 1.10: Critical Punching Perimeter for Rectangular Columns in Eurocode 2

$$u = 2 \times (c_1 + c_2) + 4\Pi d \tag{1.12}$$

Shear stress on critical punching perimeter is calculated with Equation 1.13. In Equation 1.13, ν is the shear stress on critical punching perimeter, V_u is gravity shear force on the slab column connections, u is the critical punching perimeter and d is the effective depth of the slab. β is given in Equation 1.14

$$\nu = \frac{V_u}{u \times d} \times \beta \tag{1.13}$$

$$\beta = 1 + k \times \frac{M_u}{V_u} \times \frac{u}{W} \tag{1.14}$$

In Equation 1.14, k is the coefficient which depends on column aspect ratio. It can be directly found from the table which is shown in Figure 1.11. M_u is the unbalanced moment on the slab column connections. W corresponds to shear stress distribution as a function of control perimeter, u. It is shown in Equation 1.15.

Table 1.1 Values of k for rectangular loaded areas(Eurocode 2-2003, 2003)

c_1/c_2	≤ 0,5	1,0	2,0	≥ 3,0
k	0,45	0,60	0,70	0,80

Figure 1.11: k Values for Different Column Aspect Ratios according to Eurocode 2

$$W = \frac{c_1^2}{2} + c_1 c_2 + 4 c_2 d + 16 d^2 + 2 \Pi d c_1 \quad (1.15)$$

In Equation 1.15, c_1 is the column dimension in lateral loading direction, c_2 is the column dimension in direction perpendicular to lateral loading direction. Shear stress distribution is illustrated in Figure 1.12.

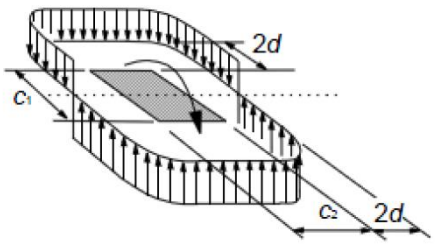

Figure 1.12: Shear Stress Distribution on Critical Punching Perimeter (Eurocode 2, 2003)

Shear strength is determined with Equation 1.16. In Equation 1.16, ρ is the flexural reinforcement ratio and it is calculated with Equation 1.17. ρ_y and ρ_z are the tension flexural reinforcement ratio in y and z direction, respectively. k is the coefficient took into account size effect and it is calculated with Equation 1.18.

$$v_{resistance} = 0.18 \times k \times (100 \times \rho \times f_c)^{\frac{1}{3}} \geq v_{min} \quad (1.16)$$

$$\rho = \sqrt{\rho_y \times \rho_z} \leq 0.02 \quad (1.17)$$

$$k = 1 + \sqrt{\frac{200}{d}} \leq 2 \quad d \text{ in } mm \quad (1.18)$$

Moment capacities of the slab-column connection is found with Equation 1.19. Equation 1.19 is derived from Equation 1.13 and Equation 1.14.

$$M_n = \frac{(v_{resistance} \times u \times d - V_u) \times W}{k \times u} \tag{1.19}$$

1.5 Objectives

Main purpose of this study is evaluating analysis methods of slab-column connections depending on rules included in Turkish Specification, TBDY 2018. In this manner, analysis methods which are eccentric shear stress model and finite element model are compared in the light of experimental test results to examine accuracy of analysis methods.

In the scope of finite element model, two different approaches investigated to obtain shear stresses on the critical punching perimeter. Effect of mesh size on the results of finite element model is also examined.

Effects of flexural reinforcement ratio on the capacity of punching shear investigated and an improvement for the eccentric shear stress model is proposed with a revised γ_v equation as a function of flexural reinforcement ratio and gravity shear ratio.

CHAPTER 2

LITARETURE REVIEW

In this chapter, some of the theoretical and experimental studies related to flat plat slab-column connections is reviewed. These studies provide the necessary background to understand the behavior of slab-column connections subjected to lateral loads. Findings and important results obtained from these studies are presented in this section.

Hanson et al. (1968) compared four different design methods investigating seventeen test specimen includes different properties such as column shape, slab geometry (with or without hole) and type of lateral loading (biaxially or uniaxially) As a result of this study, (Hanson et al, 1968)

- Design method included in ACI-ASCE Committee 326 estimated moment capacity of connection better for moment reduction factor between 0.2 and 0.4.
- Design method proposed by Moe (1961) gave good results and applied easily.
- ACI Building Code published in 1963 was applied satisfactorily to predict strength of the connection with a safety factor 2.

Ghali et al. (1976) tested six specimens under dynamic and static horizontal forces. Main scope of that study is observing the behavior of the connection under different loading conditions. Moreover, effects of flexural reinforcement ratio on strength of the connection were investigated. In this context, wide range of flexural reinforcement ratio, from %0.5 to %1.5, was used in specimens tested under static and dynamic lateral forces. Important conclusions from the work of Ghali (1976) are as follows:

- Moment capacity of the slab-column connection increased with the increasing of flexural reinforcement. Increase of the moment capacity caused to decrease of ductility of the connection and punching failure occurred very suddenly. In addition, it is observed that plastic rotation capacity of slab before punching failure decreases by increasing of flexural reinforcement.
- Increasing of moment capacity is observed dramatically up to 1% flexural reinforcement ratio. For the higher flexural reinforcement ratio, increase on the moment capacity was not so high because slab reached its punching shear capacity before flexural yielding.
- Energy absorption capacity and ductility of the system decreased by increasing the flexural reinforcement ratio. Therefore, use of high reinforcement ratios in slabs is not recommended for high ductility in seismic zones.
- Due to the strain hardening of concrete and steel rapidly, test specimen conducted with dynamic lateral forces resulted in failure on high moment compared to the test specimen conducted with static lateral forces.

Morison and Sozen (1981) conducted eight different test specimens. Three of them were tested under dynamic lateral load and five of them were tested under static lateral load. In the scope of that study, effects of gravity load and amount of flexural reinforcement were investigated. Important results are given below.

- Strength of the slab-column connections increased with increasing amount of flexural reinforcement. However, it is clearly seen that if the slab was reinforced excessively, stiffness of the connection is not as much as expected. Rotation capacity of slab is smaller than slightly reinforced concrete slab-column connection.
- Low level superimposed dead load did not decrease the strength of the connection significantly. Test specimens with low levels of superimposed dead load and without superimposed dead load gave similar results in terms of moment capacity.

- Strength of the tests conducted under dynamic lateral load was higher than strength of test specimen which have similar properties under static lateral load.

Robertson and Durani (1990) tested nine test specimens. Seven test specimens constructed with one interior and two exterior columns. Remaining two specimens were constructed as interior and exterior connection with single columns. Variables of the test specimens for interior connections were the amount gravity force, compressive strength of concrete. Flexural reinforcement ratio was same for all test specimens. Researchers conclude that (Robertson and Durani, 1990)

- Amount of unbalanced moment transferred from the column to the slab and drift capacity of the connection significantly decreased by increasing of gravity load.
- Test specimens with high gravity shear ratio failed by punching shear before reaching shear strength value recommended by ACI. Therefore, it was concluded that if the gravity shear ratio is higher than 0.3, ACI code can be unconservative.
- If direct shear stress caused by gravity load is higher than $1.2\times\sqrt{fc}$ (psi) or $0.1\times\sqrt{fc}$ (MPa), ACI code for design approach was found to be unconservative.
- Gravity shear ratio should be smaller than 0.4 for interior connections to obtain 1.5 percent drift ratio according to ACI Committee 352. Researchers suggested that gravity shear ratio should be smaller than 0.35 depending on the experimental results to ensure having enough drift capacity.
- ACI code recommended that γ_f should be taken 0.6 for square columns, however, it varied between 0.55 and 0.85 based on those experimental results. Therefore, it can be allowed using γ_f value between 0.6 and 0.8 for square column. Consequently, γ_v can be used between 0.2 and 0.4 for square columns to always provide $\gamma_f + \gamma_v = 1$

Pan and Moehle (1992) conducted four test specimens to investigate the behavior of interior slab-column connections under gravity and lateral loads. Main purposes of this study were to evaluate the effects of biaxial loading and to observe how the amount of gravity loads influence the behavior of interior slab-column connection. In this manner, two sets of specimens were tested under biaxial and uniaxial lateral load also different amount of gravity load was applied for each set of specimens. Moreover, one of test specimen was repaired and used again as a fifth test specimen to investigate strength of the connection. Some results obtained study are sorted below. (Pan and Moehle, 1992)

- Test specimens biaxially loaded have less strength compared to the test specimen loaded uniaxially as well as less stiffness, less ductility, and less capacity of drift ratio.
- Increasing the gravity load reduced the strength of the slab-column connection. In the scope of this study, analysis results of relevant test specimens by using eccentric shear stress model and finite element model are found proper with that experimental result.
- Although repairing of test specimen provided lateral drift capacity same with original test specimen, strength obtained in original test specimen didn't be provided.
- Shear strength defined in ACI 318-89, $1/3\sqrt{fc}$, was found conservative compared to both results of test specimen loaded biaxially and uniaxially.
- It was recommended that inter story drift ratio should be limited with 1.5 percent for structures subjected to high seismic force.

Farhey et al (1993) conducted four tests to investigate the failure mechanism and to observe the location of failure. In the scope of this study, influence of gravity loading and how aspect ratio affects strength of the connection were also examined. Some approaches to predict the ultimate strength of slab-column connections were compared with the experimental results such as yield line theory, eccentric shear

stress model included in ACI 318-89, ASCE-ACI 426 and beam analogy method. (Islam and Park, 1976) Some results of experiment is presented below.

- Eccentric shear stress model approach included in ACI 318-89 estimated moment capacity of connection better compared to other approaches.
- It is mentioned that number of test specimen was not enough for creating of a theoretical model to predict ultimate strength of connection. More further experiments should be conducted in the wide range of parameters like material properties, gravity load, lateral load and physical properties or combination of them.

γ_f and γ_v are calculated with Equation 1.1 and 1.5 in the current and old ACI Codes. Column aspect ratio is only parameter to estimate contribution factor of transferred moment, γ_f, calculated with Equation 1.1. However, according to experimental results it is clearly observed that even if all dimensions, material properties and loading conditions are same for the test specimen, ultimate moment capacity of the connection is changed by using different flexural reinforcement ratio. This means that how much of ultimate moment must be carried by shear capacity or flexural capacity changes depending on the flexural reinforcement ratio. Luo and Durani (1995) derived Equation 2.1 to estimate contribution factor, γ_v, of transferred moment better depending on the experimental results obtained from test specimens which have punching failure mode for gravity shear ratio is higher than 0.15. Here, γ_v was calculated back with Equation 1.6 using moment capacity of connection and gravity shear force applied in experiments. Results are shown in Figure 2.1. It was seen that γ_v decreases by increasing flexural reinforcement ratio. Then best line was fitted, and modified Equation 2.1 was derived for better prediction of γ_v. (Luo and Durani, 1995)

$$\gamma_v = 1.1 - 18\rho - \frac{1}{1 + \frac{2}{3}\sqrt{\frac{b_1}{b_2}}} \tag{2.1}$$

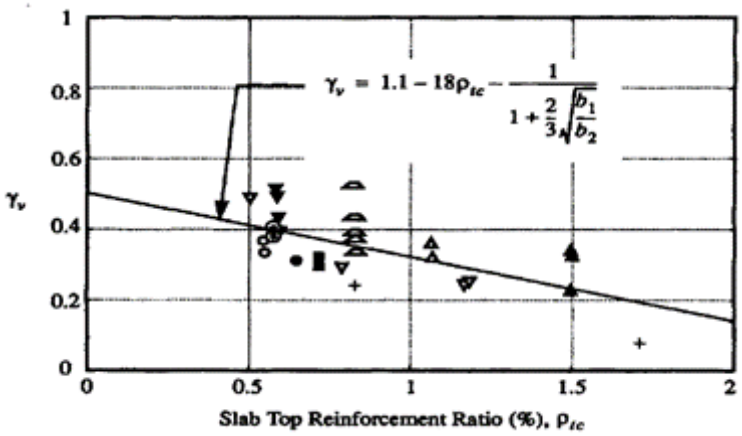

Figure 2.1 Estimation of γ_v Based on Flexural Reinforcement Ratio (Luo and Durani, 1995)

In the scope of current study, new γ_v formula are presented in Section 3.5 based on flexural reinforcement ratio and gravity shear ratio for a better prediction.

Park and Choi (2006) developed a numerical approach to analyze flat plate slab-column connections better. According to findings, developed numerical model gave better results compared to ACI 318-02 Code in the light of experimental results. Some findings are listed below:

- Contribution factor of transferred moment carried by shear, γ_v, was specified between 0.6 and 0.8 which was higher than 0.4 recommended in ACI 318-02.
- Although critical shear strength was found as $0.33\sqrt{fc}$ (MPa), torsional shear strength was specified as $1.15\sqrt{fc}$ (MPa).

Ghali and Megally (2011) studied the effects of gravity load on the drift capacity of slab-column connections. Moreover, it was investigated whether traditional strength enhancement methods such as drop panel and shear capital increase the shear strength and ductility or not. Effects of shear reinforcement was also reviewed whether it increase strength and ductility or not. As a result of this study, (Ghali and Megally, 2011)

- It is clearly seen that even if strength enhancement methods increase the strength of the connection, ductility was not provided. Moreover, stirrups did not increase the ductility of the connection significantly while it increased strength of the slab-column connection. Use of stud-shear reinforcement increased both the ductility and punching shear strength of the connection.
- Recommended value was 0.4 for the upper limit of gravity shear ratio to provide at least 1.5 percent lateral drift capacity for interior slab-column connections constructed without shear reinforcement. Gravity shear ratio was limited to 0.32 and 0.25 for 2 percent and 2.5 percent drift ratio, respectively.
- If the gravity shear ratio was smaller than 0.25, using of shear reinforcement was not needed but if this ratio was higher than 0.4 and the lateral drift capacity was smaller than 1.5 percent, use of shear reinforcement was necessary for such cases.

Choi et al. (2014) stated that specifying the contribution factor of transferred moment, γ_f carried by flexure with Equation 1.1 included in ACI did not correlate well with test results and column aspect ratio could not be an important parameter to determine this contribution factor. Therefore, a new model was proposed to estimate strength of the connections. Unlike ACI Code, new proposed model did not prescribe contribution factor of transferred moment and it employed the transferred moment directly. Important findings are summarized below. (Choi et al, 2014)

- Recommended contribution factor was 0.6 for γ_f for the eccentric shear stress model included in ACI 318-11 for square columns. However, it was stated that γ_f calculated with Equation 2.2 varied between 0.2 and 1.15 based on the experimental results. In Equation 2.2, M_F is the flexural strength of slab calculated in distance c + 3h based on rules included in ACI 318-11. Mn was the total moment capacity of the connection specified in the experiments.

$$\gamma_{f,exp} = \frac{M_F}{M_n} \tag{2.2}$$

- It was also observed that γ_f was affected by the flexural tension reinforcement ratio in addition to the column aspect ratio. Luo and Durani

(1995) derived Equation 2.1 to predict the contribution of the transferred moment resisted by shear. If it is considered that total contribution is equal to 1 as in the eccentric shear stress model, γ_f is specified with Equation 2.3. Results obtained from Equation 2.2 are plotted for square columns in Figure 2.2 and it is clearly seen that γ_f increased by increasing of flexural reinforcement ratio. Results of Equation 2.3 are also fitted into graph as a line in Figure 2.2

$$\gamma_f = 18\rho + \frac{1}{1+\frac{2}{3}\sqrt{f_c}} - 0.1 \qquad (2.3)$$

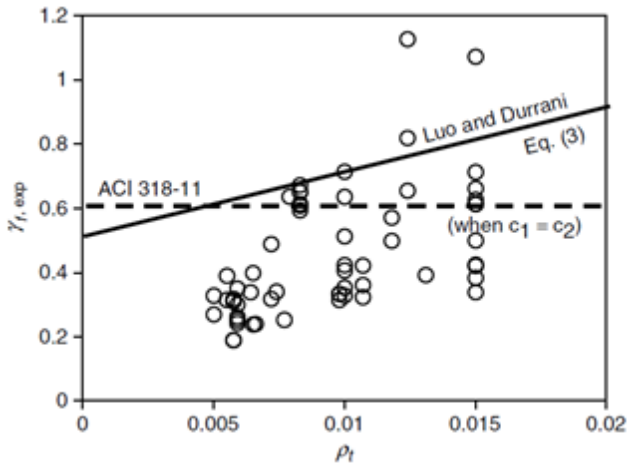

Figure 2.2 Distribution of γf on Different Flexural Reinforcement Ratio (Choi et al, 2014)

It is clearly seen that results obtained from Equation 2.3 overestimates the experimental results.

- Gravity shear ratio was defined as a critical parameter to predict contribution factor of transferred moment carried by flexure. Results obtained from Equation 2.2 were plotted for square columns in Figure 2.3 and it was observed that γ_f increased by increasing the gravity shear ratio. On the contrary, γ_v decreased by increasing the gravity shear ratio.

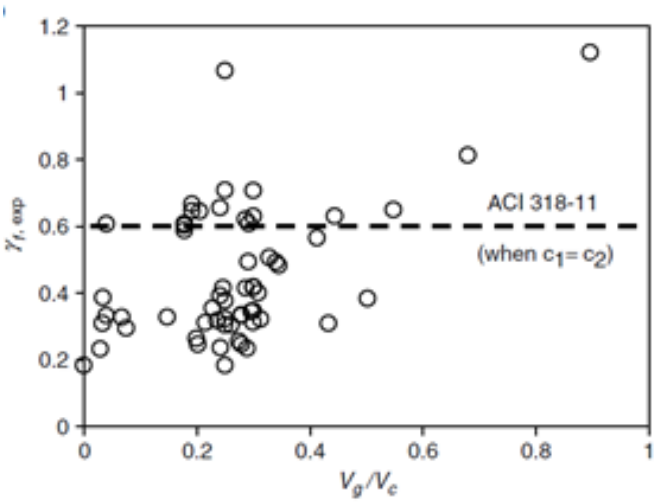

Figure 2.3 Distribution of γ_f on Different Gravity Shear Ratio (Choi et al, 2014)

- Proposed model predicted the connection strength well compared to eccentric shear stress model recommended in ACI 318-11.

In the scope of the new proposed model, amount of transferred moment capacity, M_F carried by flexural strength of slab formulated with Equation 2.4. In this equation, A_{st} and A_{sb} are the area of flexural reinforcement at top and bottom of the slab. J_{dt} and j_{db} are distance between resultant tensile force and resultant compressive force in the slab section. Yield stress of flexural reinforcement was symbolized with f_y

$$M_F = A_{st} \times f_y \times j_{dt} + A_{sb} \times f_y \times j_{db} \tag{2.4}$$

In the same section, amount of transferred moment capacity, M_V carried by shear is formulated with Equation 2.5 using eccentric shear stress model. In this equation, v_c is shear strength, v_g is shear stress caused by gravity load, J is parameter similar to the the polar moment of inertia of critical section defined in eccentric shear stress model and (c + d)/2 is distance between outermost layer of critical section and midpoint of critical section.

$$M_V = \left(v_c - v_g\right) \times \frac{J}{\frac{c+d}{2}} \tag{2.5}$$

Total moment capacity of connection specified with Equation 2.6 and Equation 2.7 and 2.8 also should be provided.

$$M_n = M_F + M_V \tag{2.6}$$

$$M_u \leq M_n \tag{2.7}$$

$$V_u \leq V_c \tag{2.8}$$

To validate the accuracy of new model proposed by Choi (2014), moment capacity ratios, $M_{n,exp}/M_{n,ACI\ 318\text{-}11}$ and $M_{n,exp}/M_{n,proposed}$ were presented with their covarience (COV). The mean value of $M_{n,exp}/M_{n,ACI\ 318\text{-}11}$ was calculated %128 with covariance of %51.1. On the other hand, mean value of $M_{n,exp}/M_{n,proposed}$ was calculated %124 with covariance of %15.3. It was observed that strength prediction of connection with ACI 318-11 was affected by variables such as flexural reinforcement ratio and gravity shear ratio, while strength prediction of conncetion with proposed method was not affected by variables dramatically.

Lots of theoretical and experimental studies were performed to understand punching failure mechanism of slab column connections. In the experimental studies, many specimens were tested to understand effects of parameters such as flexural reinforcement ratio, gravity shear ratio and column aspect ratio on punching failure mechanism of slab column connections. It was clearly observed that these parameters affects the strength of the slab column connections. In the theoretical studies, many of analitical design and finite element approaches were investigated by comparing with current design approaches such as eccentric shear stress model included in ACI 318 in the light of experimental results. However, eccentric shear stress model is still recommended as an only punching design approaches in ACI 318. However, Turkish Building Earthquake Specification allows to use finite element approach as well as eccentric shear stress model. In the scope of this study, finite element approach was investigated by comparing with experimental and eccentric shear stress model results. In addtion, simple proposal was made to improve eccentric shear stress model considering effects of variables on strength of slab column connections.

CHAPTER 3

COMPARISON OF ANALYSIS METHODS IN THE LIGHT OF EXPERIMENTAL RESULTS FOR INTERIOR REINFORCED SLAB-COLUMN CONNECTIONS

3.1 Database

A number of slab-column connections have been investigated for a long time as evidenced in the literatüre review part. There were lots of experiments conducted to understand behavior of interior and exterior flat plate slab-column connections. Reinforced concrete flat plate slab-column connections and post tensioned flat plate slab-column connections constructed with and without shear reinforcement were also investigated in these experiments.

In the scope of this study, totally forty experimental test specimens of interior reinforced slab-column connection are used as a test database. Specimens with shear reinforcement was not included in the database. Seven experimental sets of data consist of thirty test specimens were used for comparison of finite element-based design methods included in new Turkish Specification, TBDY 2018. However, thirty-two test specimens which have square columns were used to validate improvement of eccentric shear stress model. Each experimental test specimen was designated and marked at the second column in Table 3.1. Relevant parameters for the test specimens and test results are also presented in Table 3.1. Test specimens marked with A were used only for comparison of punching shear design approaches included in Turkish Specification, TBDY 2018, test specimens marked with B were used only to validate improvement of eccentric shear stress model. Test specimens marked with AB in Table 3.1 were used for both purposes. Properties of test specimens were obtained directly from Morison and Sozen (1981), Ghali (1976), Farhey (1993), Choi et al. (2014) and indirectly from Hanson and Hanson (1968),

Pan and Moehle (1992), Durani et al. (1990), Robertson and Durani (1990), fib Bulletin 81 (2016). Parameters shown in Table 3.1 are defined below.

L_1: Span length in the loading direction (mm)

L_2: Span length in the direction perpendicular to loading direction (mm)

c_1: Column dimension in the loading direction (mm)

c_2: Column dimension in the direction perpendicular to loading direction (mm)

h: Slab thickness (mm)

d: Effective depth of slab (mm)

f_c: Compressive strength of concrete (MPa)

ρ: Flexural reinforcement ratio (%)

$V_{u,exp}$: Ultimate gravitational shear force applied in experiment (kN)

$M_{n,exp}$: Measured ultimate moment before punching failure (kN.m)

Table 3.1 Parameters of Test Specimens and Results of Experiments

Researcher	Exp. No. /Marking	Specimen	L_1, mm	L_2, mm	c_1, mm	c_2, mm	h, mm	d, mm	f_c, MPa	ρ, %	$V_{u,exp}$, kN	$M_{n,exp}$, kN.m
Morison and Sozen	1AB	S1	1829	1829	305	305	76.2	61	45.8	0.65	5.83	34.23
Morison and Sozen	2AB	S2	1829	1829	305	305	76.2	61	35.1	0.98	5.83	38.75
Morison and Sozen	3AB	S3	1829	1829	305	305	76.2	61	33.9	1.31	5.83	41.13
Morison and Sozen	4AB	S4	1829	1829	305	305	76.2	61	34.9	0.98	14.3	35.48
Morison and Sozen	5AB	S5	1829	1829	305	305	76.2	61	35.2	0.98	28.6	37.51
Hanson and Hanson	6AB	A12	1829	1219	152	152	76.2	57.2	33.2	1.5	26.87	20.45
Hanson and Hanson	7AB	A13L	1829	1219	152	152	76.2	57.2	32.8	1.5	26.16	19.89
Hanson and Hanson	8A	B16	1829	1219	305	152	76.2	57.2	30.4	1.5	34.38	27.34
Hanson and Hanson	9A	C17	1829	1219	152	305	76.2	57.2	36	1.5	31.49	24.74
Pan and Moehle	10AB	1	3658	3658	274	274	121.9	103.4	33.3	0.72	103.64	74.8
Pan and Moehle	11A	3	3658	3658	274	274	121.9	103.4	31.4	0.72	62.72	105.53
Durani et al.	12AB	DNY1	2896	1981	254	254	114.3	96.8	35.3	0.59	54.27	47.23
Durani et al.	13AB	DNY2	2896	1981	254	254	114.3	96.8	25.7	0.59	68.06	33.44
Durani et al.	14AB	DNY3	2896	1981	254	254	114.3	96.8	24.6	0.59	54.27	48.36
Durani et al.	15AB	DNY4	2896	1981	254	254	114.3	96.8	19.1	0.59	54.27	44.06
Robertson and Durani	16AB	1	2896	1981	254	254	114.3	96.8	38	0.83	53.38	64.74
Robertson and Durani	17AB	2C	2896	1981	254	254	114.3	96.8	33	0.83	53.38	66.21
Robertson and Durani	18AB	3SE	2896	1981	254	254	114.3	96.8	44	0.83	53.38	72.31
Robertson and Durani	19AB	4S	2896	1981	254	254	114.3	96.8	43.9	0.83	53.38	74
Robertson and Durani	20AB	5SO	2896	1981	254	254	114.3	96.8	38	0.83	53.38	66.77
Robertson and Durani	21A	6LL	2896	1981	254	254	114.3	96.8	32.2	0.83	129.44	25.65
Robertson and Durani	22AB	7L	2896	1981	254	254	114.3	96.8	30.8	0.83	92.52	39.88
Robertson	23AB	8I	2896	1981	254	254	114.3	91.2	39.3	0.83	47.15	66.66
Ghali at al.	24AB	SM0.5	1830	1830	305	305	152	121	36.8	0.5	129	100
Ghali at al.	25AB	SM1.0	1830	1830	305	305	152	121	33.4	1	129	128
Ghali at al.	26AB	SM1.5	1830	1830	305	305	152	121	40	1.5	129	133
Farhey at al.	27A	1	2690	2690	300	200	80	59.7	35.1	0.58	0	32.99
Farhey at al.	28A	2	2690	2690	300	200	80	59.7	35.1	0.58	0	32.99
Farhey at al.	29A	3	2690	2690	300	200	80	59.7	15	0.58	24.91	18.98
Farhey at al.	30A	4	2690	2690	300	120	80	59.7	15	0.58	24.91	15.03
Luo and Durani	31B	I.I	2896	1981	254	254	114.3	96.8	20.7	0.59	15.44	39.32
Luo and Durani	32B	INT1	3048	2896	254	254	114.3	96.8	30.9	0.55	108.98	39.21
Luo and Durani	33B	INT2	3048	2896	254	254	114.3	96.8	30.7	0.55	125.88	31.64
Islam and Park	34B	1	2743	2286	229	229	88.9	88.9	27.3	1.07	35.76	30.51
Islam and Park	35B	2	2743	2286	229	229	88.9	88.9	31.9	1.07	35.76	37.74
Islam and Park	36B	3C	2743	2286	229	229	88.9	88.9	29.7	1.07	35.76	35.82
Hawkins et al.	37B	S1	3658	2134	305	305	152.4	114.3	34.8	1.18	128.11	144.62
Hawkins et al.	38B	S2	3658	2134	305	305	152.4	117.6	23.4	0.79	142.34	87.9
Hawkins et al.	39B	S3	3658	2134	305	305	152.4	120.7	22.1	0.51	138.78	53.67
Hawkins et al.	40B	S4	3658	2134	305	305	152.4	114.3	32.3	1.18	149.9	125.41

In the database, different kind of test specimens are included in terms of parameters such as compressive strength, flexural reinforcement, dimensions of column, slab thickness, amount of gravitational shear force. Test parameters with number of tests are shown in Figure 3.1, 3.2 and 3.3 for group of test specimens marked with A and AB. Compressive strength for group of test specimens marked with A and AB varies between 15 MPa to 45.8 MPa and %83 of them is in a specific range between 25 MPa and 45 MPa. Minimum and maximum flexural reinforcement ratio are %0.5 and %1.5, respectively, but major part of test specimen reinforced with ratio between %0.5 and %1. Effective depth of slab alters from 57.2 mm and 121 mm.

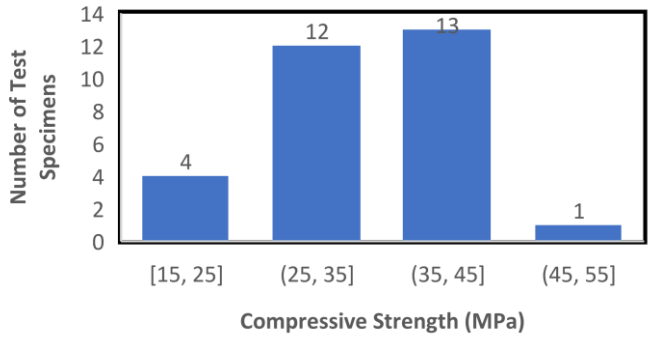

Figure 3.1 Distribution of Compressive Strength for Group of Test Specimens Marked with A and AB

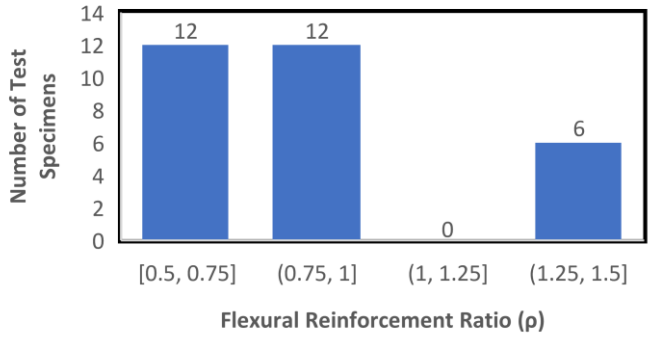

Figure 3.2 Distribution of Flexural Reinforcement Ratio for Group of Test Specimens Marked with A and AB

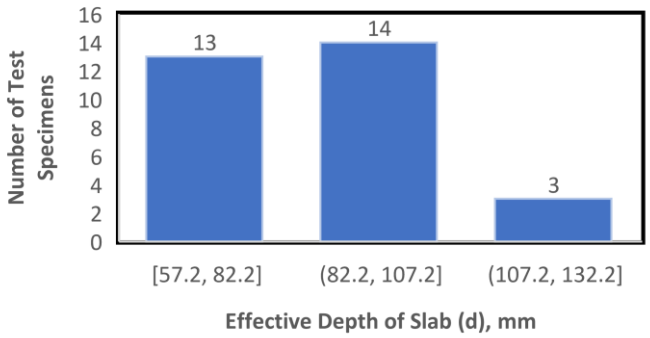

Figure 3.3 Distribution of Effective Depth of Slab for Group of Test Specimens Marked with A and AB

Distributions of parameters for group of test specimens marked with AB and B is summarized in Figure 3.4, 3.5 and 3.6.

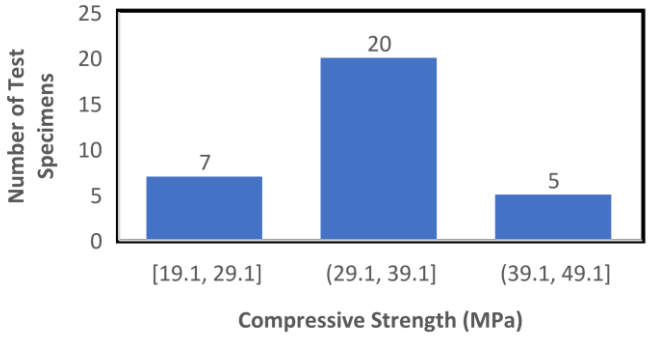

Figure 3.4 Distribution of Compressive Strength for Group of Test Specimens Marked with AB and B

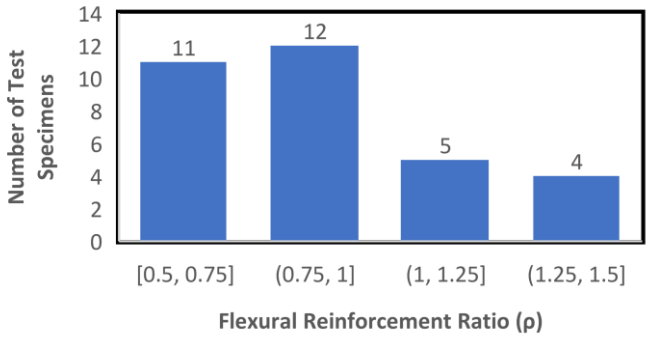

Figure 3.5 Distribution of Flexural Reinforcement Ratio for Group of Test Specimens Marked with AB and B

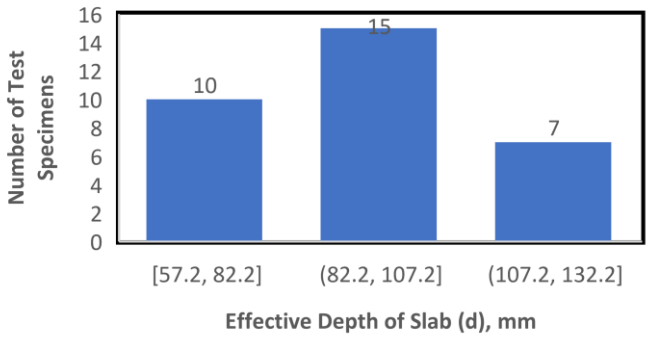

Figure 3.6 Distribution of Effective Depth of Slab For Group of Test Specimens Marked with AB and B

In the group of test specimens market with AB and B, compressive strength varies between 19.1 MPa to 45.8 MPa. Minimum and maximum flexural reinforcement ratios are %0.5 and %1.5, respectively, but major part of test specimen has flexural reinforcement ratio between %0.5 and %1. Effective depth of slab alters from 57.2 mm and 121 mm.

3.2 Method 1: Eccentric Shear Stress Model

Eccentric shear stress model was explained in detail previously in Section 1.3.1. In this section, moment capacities of interior slab-column connections are calculated using the eccentric shear stress model for the group of test specimens marked with A and AB. Then, results are compared with the experimental results to assess the accuracy of the eccentric shear stress model in predicting the moment capacity of the slab-column connections.

In the scope of the eccentric shear stress model, shear stress obtained from Equation 1.6 must be smaller than shear strength of concrete which is determined similar to the tensile strength of concrete in the Turkish Specification. Shear strength equation is given in Equation 3.1 taken from Turkish Specification, TS 500. If the shear stress finding from Equation 1.6 is smaller than shear strength which is calculated from Equation 3.1, shear reinforcement is not needed, and slab-column connection is safe

in terms of punching. If shear stress is higher than shear strength, shear reinforcement should be used, or slab-column connection must be strengthened.

$$f_{ctd} = 0.35\sqrt{f_c} \tag{3.1}$$

Therefore, shear strength obtained from Equation 3.1 is accepted as a maximum shear stress on the slab before failure of slab designed without shear reinforcement. Moment capacity of connection is calculated by using Equation 3.2 derived from Equation 1.6 by assuming a shear stress equal to the shear strength of concrete.

$$M_{n,ESSM} = \frac{\left(f_{ctd} - \frac{V_u}{A_c}\right) \times J_c}{\gamma_v \times c} \tag{3.2}$$

Critical punching area, A_c, parameter similar to the polar moment of inertia of the critical zone, j_c, the ratio of transferred moment carried by shear, γ_v, and the distance between outer layer and midpoint of the perimeter, c, were calculated by using equations from Equation 1.1 to Equation 1.11. V_u is directly taken from the experiments. Moment capacities predicted by using the eccentric shear stress model for the group of test specimens marked with A and AB are given in Table 3.2. In addition to the moment capacities, some necessary parameters used to apply the eccentric shear stress model are also given in Table 3.2. Experimental results already given in Table 3.1, not shown in Table 3.2. Ratio of the measured moment capacity in the experiments to calculated moment capacity with eccentric shear stress model, $M_{n,exp}/M_{n,ESSM}$ are shown in Table 3.2. Subsequently, moment capacities, $M_{n,exp}$ and $M_{n,ESSM}$, and moment capacity ratios, $M_{n,exp}/M_{n,ESSM}$, are plotted in Figures 3.7 to 3.20 seperately for all experiment sets. Results are also shown together for group of test specimens marked with A and AB in Figure 3.21 and Figure 3.22. Distribution of $M_{n,exp}/M_{n,ESSM}$ results in a specific range is also shown in Figure 3.23. In addition, results for all set of experiment are summarized separately in terms of moment capacity ratio, $M_{n,exp}/M_{n,ESSM}$ as an average in Table 3.3.

It can be observed that the mean value of the moment capacity ratios, $M_{n,exp}/M_{n,ESSM}$, for set of experiments marked with A and AB varied between %69 and %139. Mean

value of the moment capacity ratios, $M_{n,exp}/M_{n,ESSM}$, is %96 with standard deviation of %26. If moment capacity ratio, $M_{n,exp}/M_{n,ESSM}$, is higher than %100, eccentric shear stress model underestimates moment capacity and gives safe results, otherwise it overestimates moment capacity and gives unsafe results. In this context, while eccentric shear stress model gives conservative results (Hanson and Hanson 1968; Pan and Moehle 1992; Ghali et al. 1976), it gives unconservative results for other datasets (Morison and Sozen 1981; Robertson and Durani 1990; Durani et al 1992; Farhey et al 1993).

Parameters are shown in Table 3.2 are defined below.

f_{ctd}: Shear strength (MPa)

u_p: Punching perimeter (mm)

A_c: Critical punching area (mm^2)

J_c: Parameter similar to the polar moment of inertia of critical zone

γ_v: The ratio of unbalanced moment carried by shear

γ_f: The ratio of unbalanced moment carried by flexure

$V_{u,exp}/V_{n,ESSM}$: Gravity shear ratio

$M_{u,exp}/M_{n,ESSM}$: The ratio of measured moment to calculated moment

Table 3.2 Eccentric Shear Stress Model Results

Researcher	Experiment	Specimen	$f_{ctd,TBDY}$, MPa	u_p, mm	A_c, mm^2	J_c, mm^4	γ_f	γ_v	$V_{u,exp}/V_{n,ESSM}$ (%)	$M_{u,exp}/M_{n,ESSM}$ (%)
Morison and Sozen	1	S1	2.37	1464	89304	2007646945	0.6	0.4	3	54
Morison and Sozen	2	S2	2.07	1464	89304	2007646945	0.6	0.4	3	70
Morison and Sozen	3	S3	2.04	1464	89304	2007646945	0.6	0.4	3	76
Morison and Sozen	4	S4	2.07	1464	89304	2007646945	0.6	0.4	8	68
Morison and Sozen	5	S5	2.08	1464	89304	2007646945	0.6	0.4	15	78
Hanson and Hanson	6	A12	2.02	837	47865	355657394	0.6	0.4	28	165
Hanson and Hanson	7	A13L	2	837	47865	355657394	0.6	0.4	27	160
Hanson and Hanson	8	B16	1.93	1143	65368	1249207715	0.53	0.47	27	132
Hanson and Hanson	9	C17	2.1	1143	65368	547162706	0.66	0.34	23	98
Pan and Moehle	10	1	2.02	1510	156093	3774935300	0.6	0.4	33	110
Pan and Moehle	11	3	1.96	1510	156093	3774935300	0.6	0.4	20	135
Durani et al.	12	DNY1	2.08	1403	135830	2838914427	0.6	0.4	19	69
Durani et al.	13	DNY2	1.77	1403	135830	2838914427	0.6	0.4	28	65
Durani et al.	14	DNY3	1.74	1403	135830	2838914427	0.6	0.4	23	89
Durani et al.	15	DNY4	1.53	1403	135830	2838914427	0.6	0.4	26	96
Robertson and Durani	16	1	2.16	1403	135830	2838914427	0.6	0.4	18	91
Robertson and Durani	17	2C	2.01	1403	135830	2838914427	0.6	0.4	20	101
Robertson and Durani	18	3SE	2.32	1403	135830	2838914427	0.6	0.4	17	93
Robertson and Durani	19	4S	2.32	1403	135830	2838914427	0.6	0.4	17	95
Robertson and Durani	20	5SO	2.16	1403	135830	2838914427	0.6	0.4	18	94
Robertson and Durani	21	6LL	1.99	1403	135830	2838914427	0.6	0.4	48	61
Robertson and Durani	22	7L	1.94	1403	135830	2838914427	0.6	0.4	35	78
Robertson	23	8I	2.19	1381	125929	2544654890	0.6	0.4	17	99
Ghali at al.	24	SM0.5	2.12	1704	206184	6362022095	0.6	0.4	29	89
Ghali at al.	25	SM1.0	2.02	1704	206184	6362022095	0.6	0.4	31	123
Ghali at al.	26	SM1.5	2.21	1704	206184	6362022095	0.6	0.4	28	112
Farhey at al.	27	1	2.07	1239	73956	1478814818	0.56	0.44	0	85
Farhey at al.	28	2	2.07	1239	73956	1478814818	0.56	0.44	0	85
Farhey at al.	29	3	1.36	1239	73956	1478814818	0.56	0.44	25	100
Farhey at al.	30	4	1.36	1079	64404	1169845611	0.51	0.49	29	116

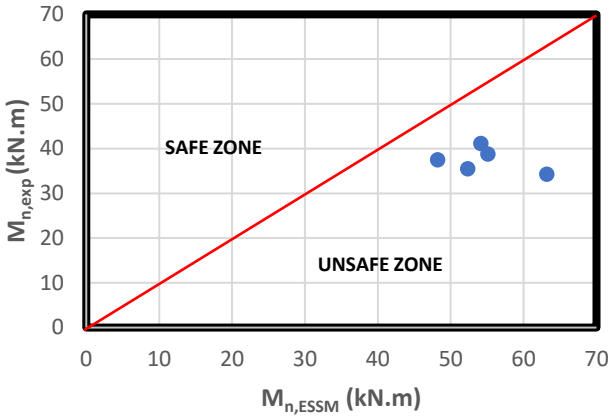

Figure 3.7 Comparison of Moment Capacity (Morison and Sozen, 1981)

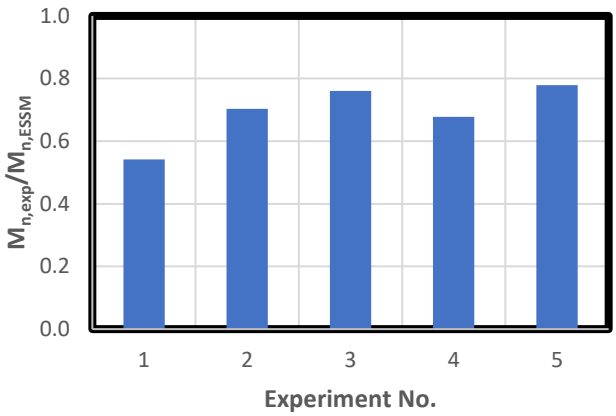

Figure 3.8 Moment Capacity Ratios, $M_{n,exp}/M_{n,ESSM}$ (Morison and Sozen, 1981)

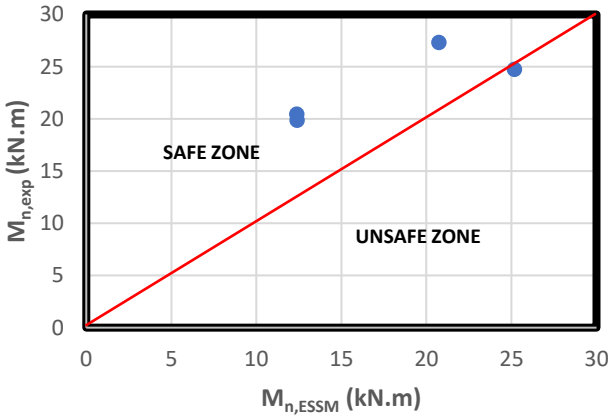

Figure 3.9 Comparison of Moment Capacity (Hanson and Hanson, 1968)

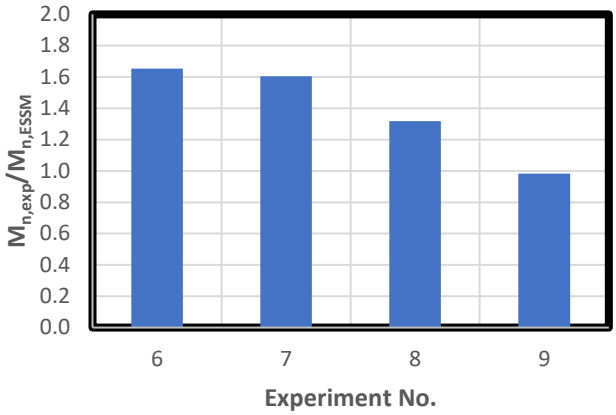

Figure 3.10 Moment Capacity Ratios, $M_{n,exp}/M_{n,ESSM}$ (Hanson and Hanson, 1968)

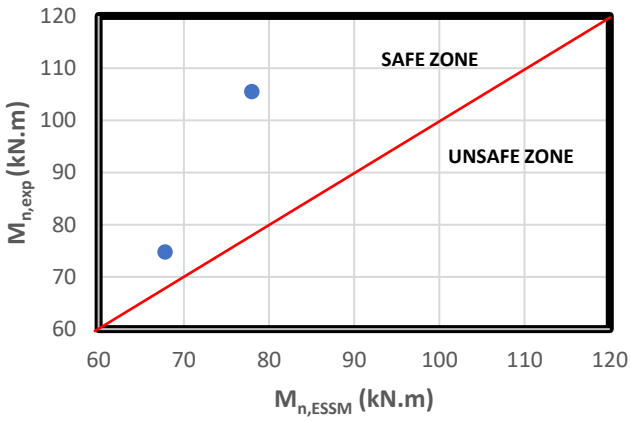

Figure 3.11 Comparison of Moment Capacity (Pan and Moehle, 1992)

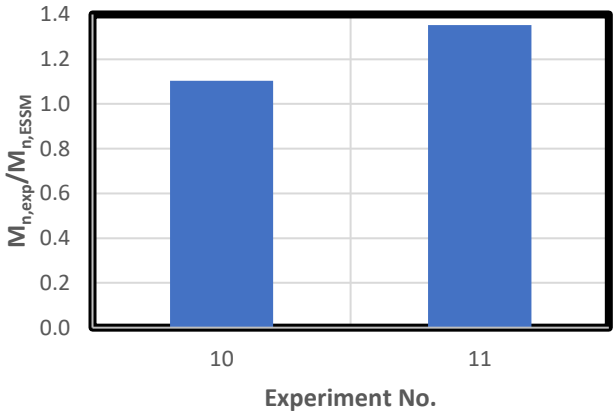

Figure 3.12 Moment Capacity Ratios, $M_{n,exp}/M_{n,ESSM}$ (Pan and Moehle, 1992)

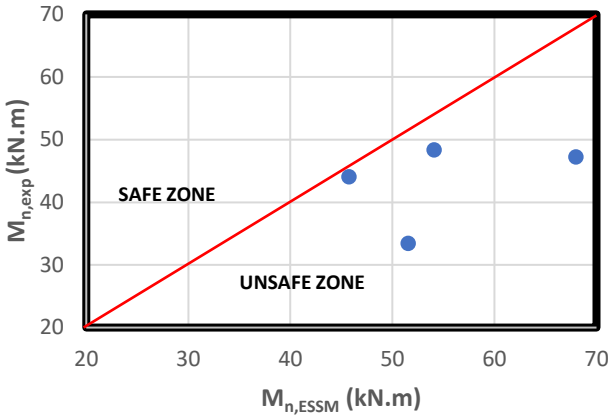

Figure 3.13 Comparison of Moment Capacity (Durani et al., 1995)

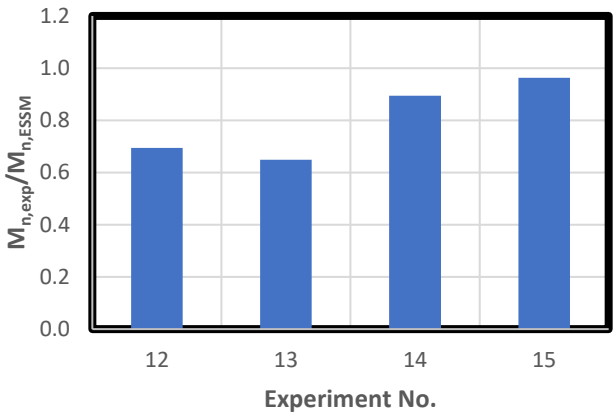

Figure 3.14 Moment Capacity Ratios, $M_{n,exp}/M_{n,ESSM}$ (Durani et al., 1995)

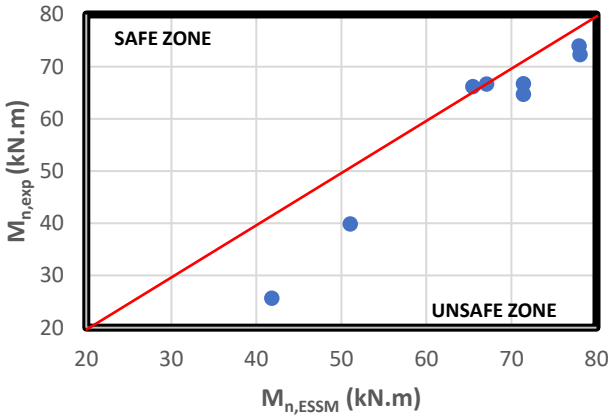

Figure 3.15 Comparison of Moment Capacity (Robertson and Durani, 1990)

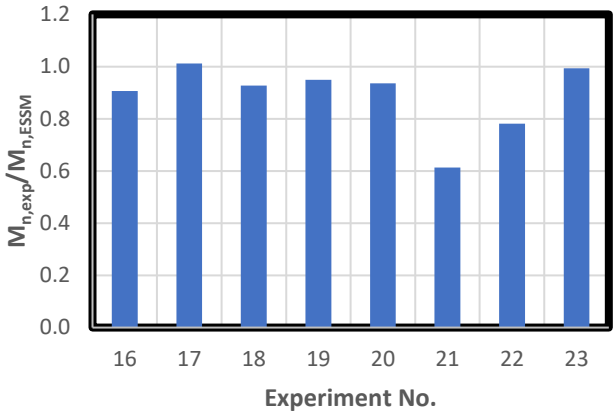

Figure 3.16 Moment Capacity Ratios, $M_{n,exp}/M_{n,ESSM}$ (Robertson and Durani, 1990)

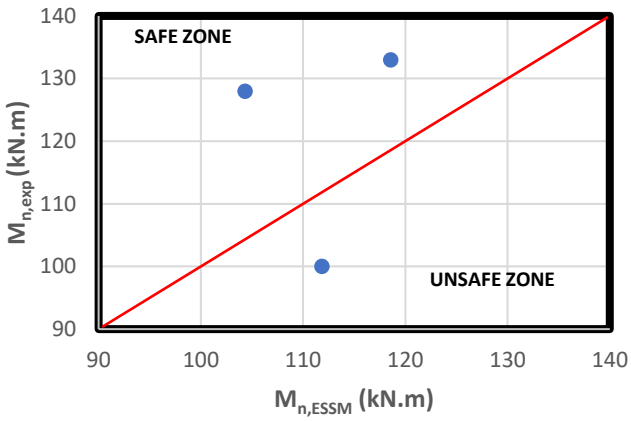

Figure 3.17 Comparison of Moment Capacity (Ghali et al., 1976)

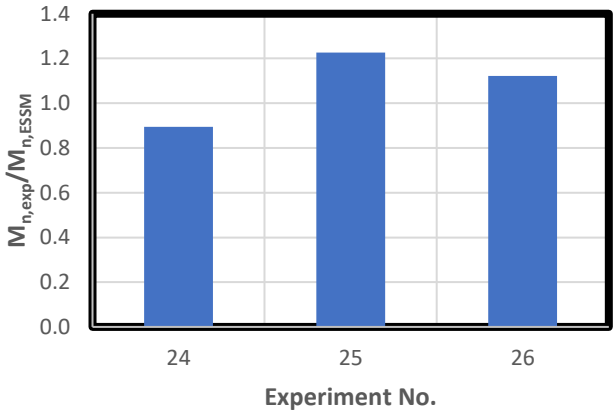

Figure 3.18 Moment Capacity Ratios, $M_{n,exp}/M_{n,ESSM}$ (Ghali et al., 1976)

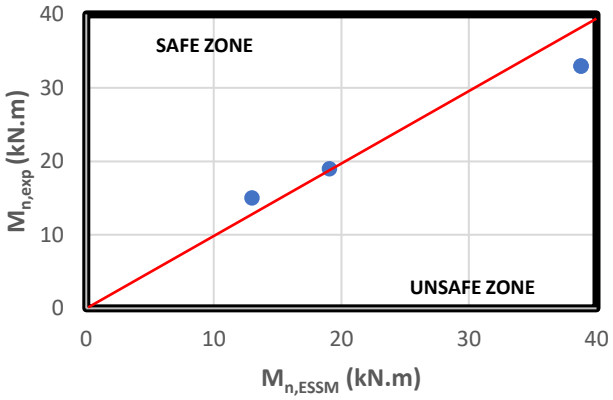

Figure 3.19 Comparison of Moment Capacity (Farhey et al., 1993)

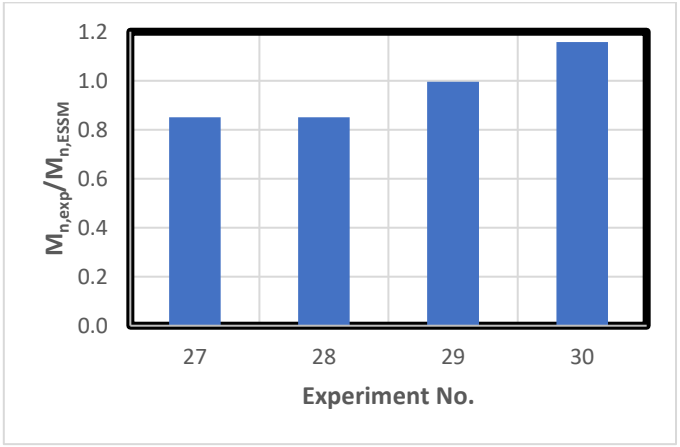

Figure 3.20 Moment Capacity Ratios, $M_{n,exp}/M_{n,ESSM}$ (Farhey et al., 1993)

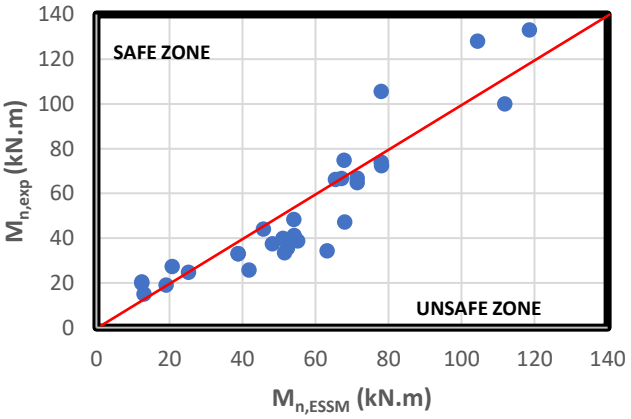

Figure 3.21 Comparison of Moment Capacity for the Group of Test Specimens Marked with A and AB

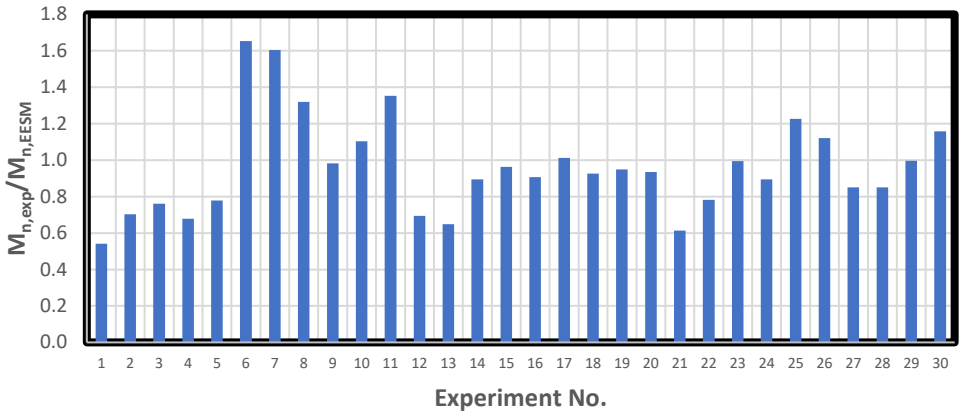

Figure 3.22 Moment Capacity Ratios, $M_{n,exp}/M_{n,ESSM}$ For the Group of Test Specimens Marked with A and AB

Table 3.3 Comparison of Experimental Results and Eccentric Shear Stress Model Results

Researcher	Mean value of $M_{n,\,exp}/M_{n,ESSM}$ (%)	Standard Deviation of Results (%)
Morison and Sozen (1981)	69	8
Hanson and Hanson (1968)	139	27
Pan and Moehle (1992)	123	12
Durani and Duo (1995)	80	13
Robertson and Durani (1990)	89	12
Ghali (1976)	108	14
Farhey (1993)	96	13
Average	96	26

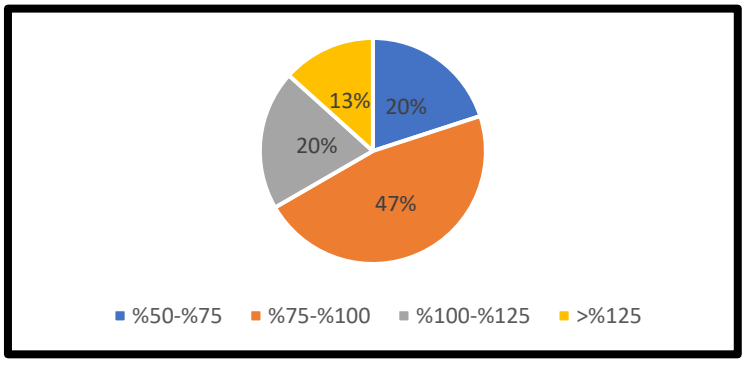

Figure 3.23 Distribution of $M_{n,exp}/M_{n,ESSM}$ Results

3.3 Method 2: Finite Element Model

Test specimens were modelled as a single interior slab-column connection in LARSA 4D. In the finite element models, slab was modelled with shell elements and column was modelled with frame elements. Typical view of a finite element model meshed with element size of d/2 is shown in Figure 3.24. Important shell elements at a distance d/2 far away from column face and at a distance d far away from column face are colored with blue and yellow, respectively, in Figure 3.24. Shell elements located in the column zone was colored with green. All column and slab dimensions were taken to be similar with parameters shown at Table 3.1.

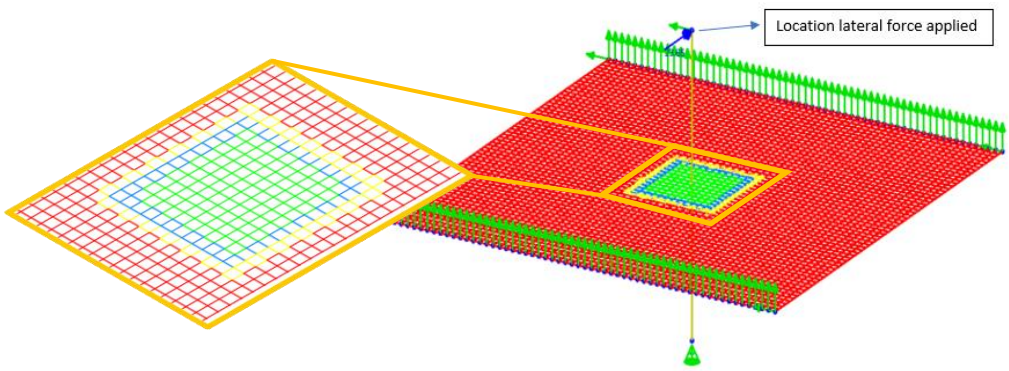

Figure 3.24 Typical View of Finite Element Models

Roller supports were defined at the edge side of the slab in the loading direction to simulate contraflexure point of slabs. Additionally, movement of the slab to the direction perpendicular to loading was restricted with defining support on the corner of slab to prevent encountering unstable results. Column is also restricted at the top and bottom to simulate contraflexure point of column similar to the experimental test specimen. Pin support was defined at the bottom of the column to prevent movement of column in both loading direction and direction perpendicular to loading similar to the experiments. Joint at the top of column is only restricted in the direction perpendicular to the loading as in the experiments to apply lateral force as illustrated

in Figure 3.24. Some examples of experimental setup of test specimen are illustrated in Figure 3.25 and Figure 3.26. Even if some experiments conducted with different setup such as in Figure 3.26, all models were created in accordance with experimental setup similar to Figure 3.25 owing to the fact that the connection demands were actually represented.

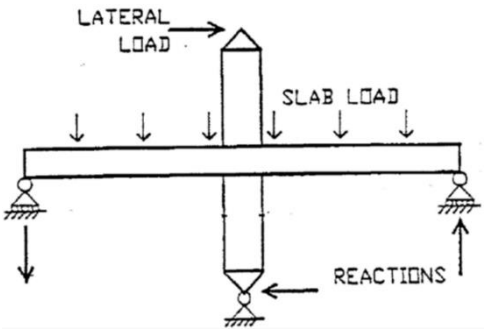

Figure 3.25 Experimental Setup of Test Specimen (Robertson and Durani 1990)

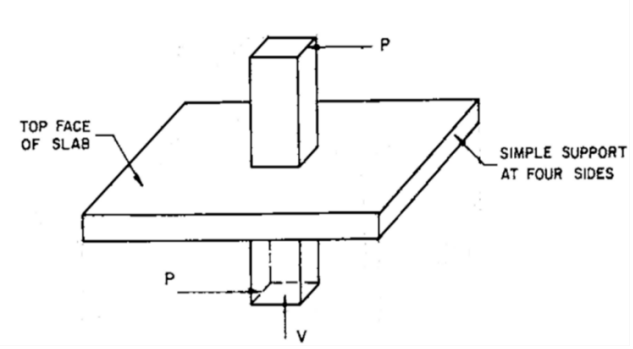

Figure 3.26 Experimental Setup of Test Specimen (Ghali et al. 1976)

Shell elements located at column zones colored with green in Figure 3.23 were defined as a rigid member. In addition, unit weight of the shell elements in this zone was taken zero because unit weight was separately defined for column frame elements. Slab thickness can be increased, or high modulus of elasticity can be defined for shell elements located at column zone to provide rigidity. First option was chosen, and slab thickness increased. Elastic modulus of concrete was calculated with Equation 3.3 included in Turkish Specification, TS 500.

$$E_c = 3250\sqrt{f_c} + 14000 \tag{3.3}$$

Crack section properties were defined for slab shell elements by decreasing modulus of elasticity apart from shell elements located in column zone. In Turkish Specification, TBDY 2018 recommended coefficient of crack section is 0.25 for slab member, however, Pan and Moehle (1992) recommended this value equal to $E_c/3$. $0.3E_c$ was preferred as the crack section property for shell elements. Poissons' ratio, ν of concrete was taken as 0.2 and shear modulus symbolized with G were calculated by using Equation 3.4. Shear modulus of uncracked section was defined to shell elements as recommended in Turkish Specification.

$$G = \frac{E_c}{2 \times (1 + \nu)} \tag{3.4}$$

Crack section property is not important for column member because moment capacity of connection specified based on resistance of slab on the connection. If the slab stiffness is same, amount of moment capacity is same. This means that, amount of lateral force is same because finite element models are analyzed statically as the experiments. Eccentricity of the dead load on the connection between slab and column exactly increase by decreasing stiffness of column but moment caused by eccentricity of dead load is very small compared to moment caused by lateral force. So, it was ignored, and uncracked section property was used for the columns.

Unit weight of concrete was taken 23.5 kN/m^3. After applying unit weight which is equal to 23.5 kN/m^3, additional distributed load was applied on the slab shell elements. Implementation of the additional gravity load or superimposed dead load is shown in Figure 3.27. All additional vertical forces were applied as a distributed load on the slab. Amount of gravity force usually is found from load cell placed at the bottom of the column in the experiments. Hence, while arranging the gravity force for the finite element model, values were obtained from the joints of pin support at the bottom of column. Staged construction analysis was used in LARSA 4D. Test specimen constructed, and only self-weight was applied in the first step. Then, if there is a superimposed dead load in the experiment, it was applied in the

second step and amount gravity force equalized with measured one in the experiment.

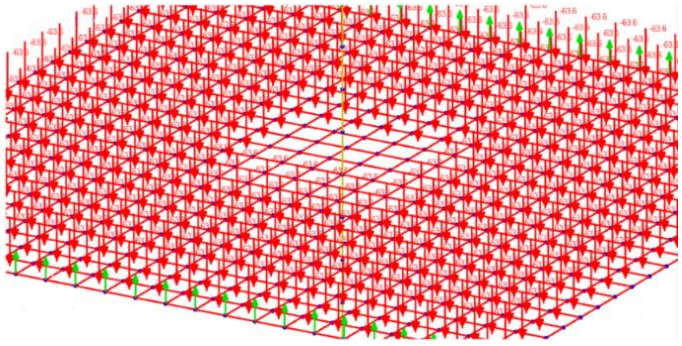

Figure 3.27 Implementation of Additional Vertical Load on Finite Element Models

Lateral force was applied as in the experiments at the top of the column in the final step. Amount of lateral load is arranged manually to find critical shear stress on the perimeter. Therefore, critical lateral force is found iteratively until observing critical shear strength value as a shear stress on the perimeter. In finite element program, shear stresses are not obtained directly. The analysis model provides shear stresses as shear force on the shell element for unit length width. Therefore, if shear stress is desired, shear force must be divided by the effective depth of slab in accordance with Turkish Specification as it is shown in Equation 1.11. Engineers should be careful at this point. If they obtain shear stress dividing by slab thickness itself, results will change significantly. As a result of the analysis, it was seen that using slab thickness as denominator in Equation 1.11 change in the results were %20. If direct shear increases by increasing of gravity shear ratio, it is seen that moment capacity of the connection changes more than %20.

Mesh size was chosen as d/2 for all the finite element models. The effect of mesh size was later studied. Shear stresses on the perimeter were computed by taking average of the shear stresses on shell elements at the right and left side of perimeter line. Two different approaches were used to determine the shear stresses on the perimeter. In the first approach, mean value of shear stresses on the shell elements inside of the perimeter and outside of the perimeter in the same line were averaged to compute the shear stress. Typical shear stress distribution on the perimeter line is

shown in Figure 3.28. Shear stress distribution on the perimeter line at the critical side is plotted in Figure 3.29. Finite elements model results show that shell element at the corner of the column which is the second shell element from the perimeter line has the highest shear stress and shear stress decreases towards the middle part of critical perimeter line. The highest stress element is taken on the critical location to determine the onset of punching failure for approach 1.

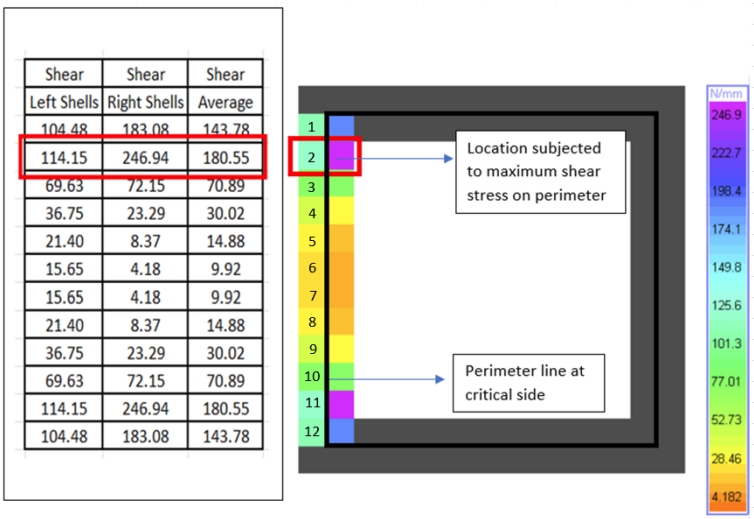

Figure 3.28 Critical Shear Stress on Punching Perimeter (Approach 1)

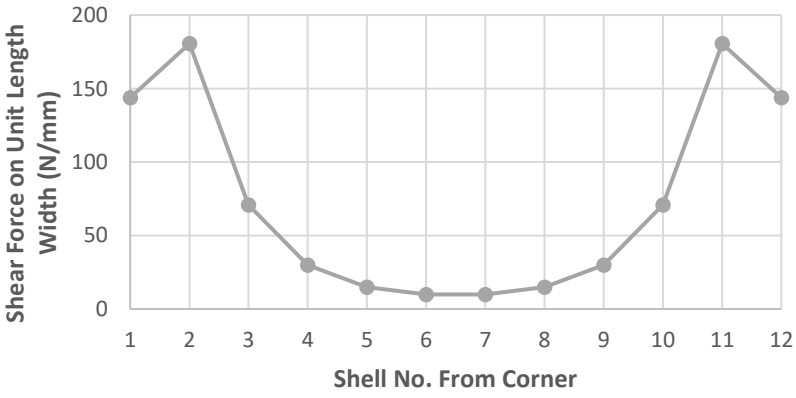

Figure 3.29 Typical Shear Stress Distribution on Critical Punching Perimeter Line

In the second approach, critical side of connection is considered as a whole, and the system pushed laterally until obtaining the critical average shear stress along the critical perimeter line. The method to obtain critical shear stress on perimeter line at

critical side is illustrated in Figure 3.30. Here, important thing is width of the mesh on the perimeter line should be equal as far as column dimension allow. Otherwise, taking the average of shear forces obtained from shell elements directly on the critical perimeter line doesn't provide accurate results. Size of mesh width also must be considered at this time while taking an average. Stress distribution and critical shear stress as an average for whole critical perimeter line is also illustrated in Figure 3.31. In short, approach 2 employs the average shear stress to estimate the onset of punching failure.

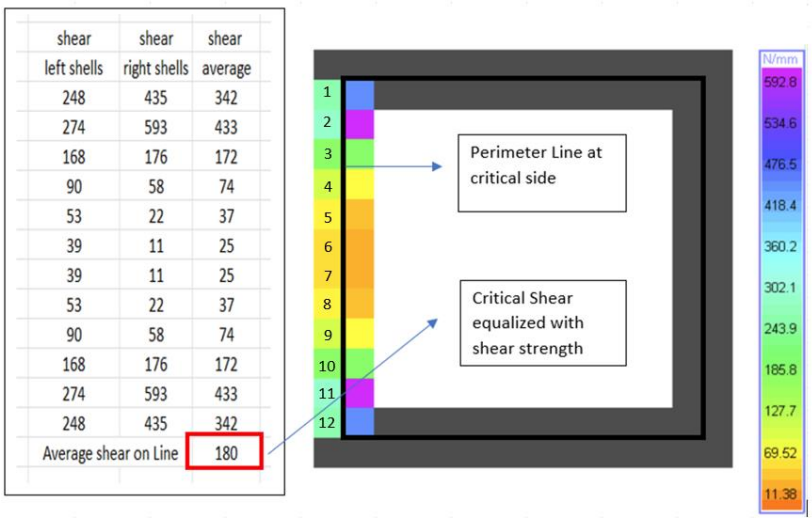

Figure 3.30 Critical Shear Stress on Critical Punching Perimeter (Approach 2)

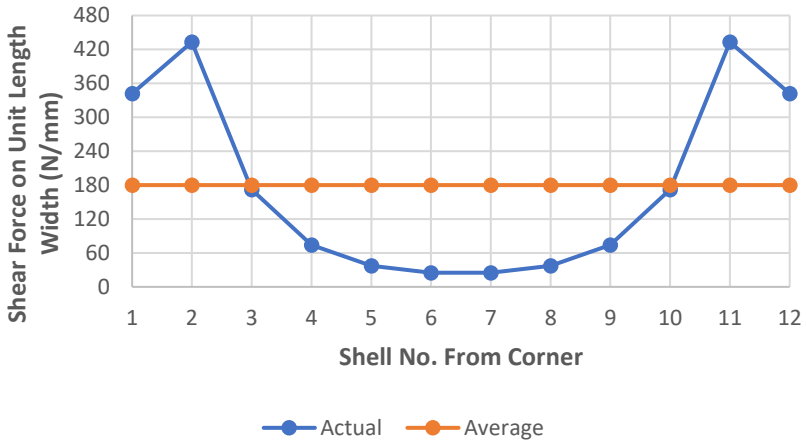

Figure 3.31 Actual and Average Shear Stress Distribution on Critical Punching Perimeter Line

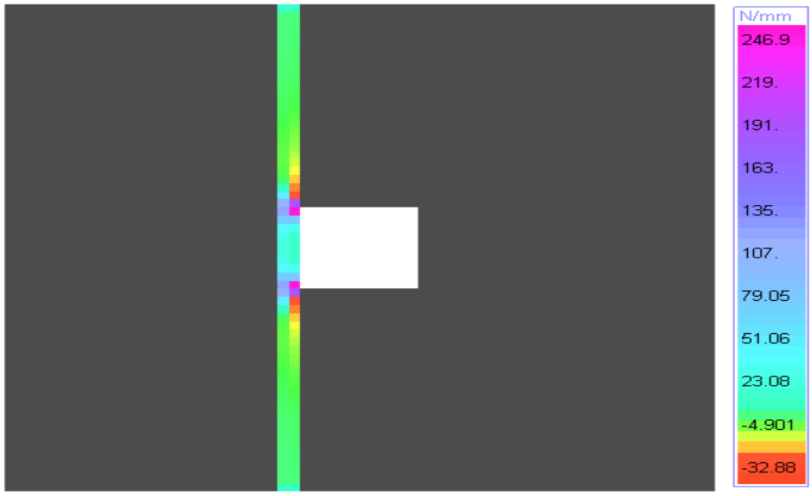

Figure 3.32 Typical Shear Stress Distribution at a Distance d from the Column Face Along the Width of the Slab

Typical shear stress distribution along the width of the slab is also shown in Figure 3.32. After obtaining of critical shear stress equal to shear strength on the perimeter line for both approaches, moment capacity of the connection was determined. As shown in Figure 3.33, total moment capacity of connection was found by summing the moment on the column at top side and bottom side of the slab. Simplified free body diagram of column ignoring moment caused by eccentricity of dead load is shown in Figure 3.34. Results for approach 1 and approach 2 are shown in Section 3.3.1 and Section 3.3.2, respectively.

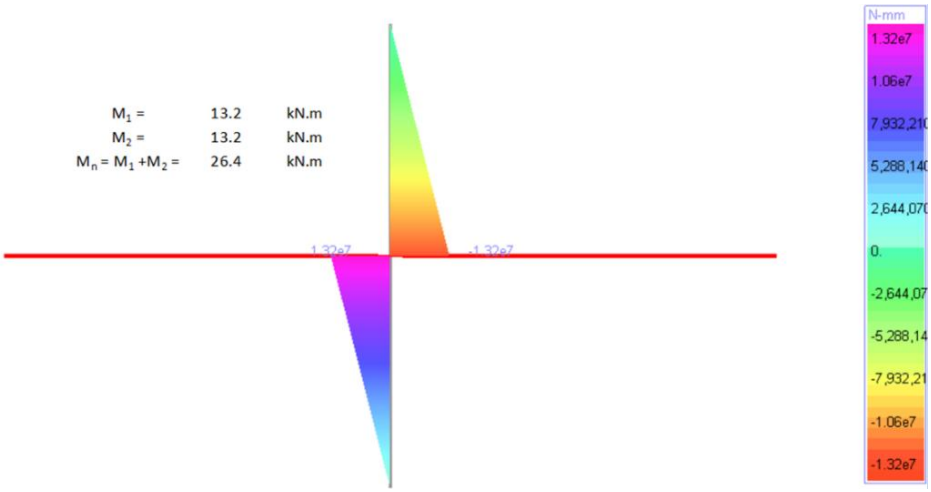

Figure 3.33 Specifying Moment Capacity of Connection

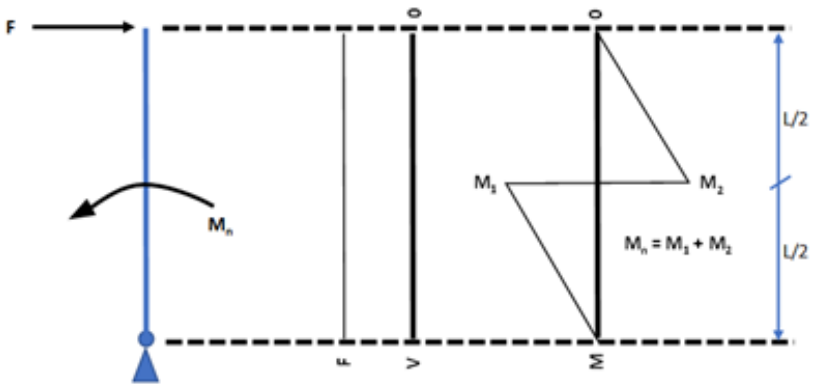

Figure 3.34 Simplified Free Body Diagram of Column

3.3.1 Approach 1 (FEM1): Maximum Shear Stress Based Design

After analysis of 30 experimental slab-column connections included in group of test speciemens marked with A and AB, it is clearly seen that approach 1 gives conservative results in the light of experimental results. Moment capacities and moment capacity ratios obtained from finite element model for all test specimen are given in Table 3.4 with some parameters used in finite element models such as modulus elasticity, E_c, modulus elasticity for cracked section, E_{cr} and shear modulus, G. Results are also shown in Figures 3.35 to 3.48 seperately for all test specimens. They are also shown in Figures 3.49 and 3.50 together for the thirty test specimens. As it is seen in Table 3.5, mean value of moment capacity ratios, $M_{n,exp}/M_{n,FEM1}$ obtained from each set of data fluctuated between %143 and %347. Mean value is also equal to %220 with a standart deviation %77 for thirty test specimen. So, even if using of this approach in design process provides safe results, it results in overdesign with a high cost of design. This requires high amount of shear reinforcement, hence it is not deemed suitable.

Table 3.4 Finite Element Model Results for Approach 1

Researcher	Experiment No.	Specimen	f_{ctd}, MPa	E_c, MPa	E_{cr}, MPa	G, MPa	$M_{n,FEM1}$, kN.m	$M_{u,exp}/M_{n,FEM1}$ (%)
Morison and Sozen	1	S1	2.37	35995	10798	14998	21.00	163
Morison and Sozen	2	S2	2.07	33255	9976	13856	18.30	212
Morison and Sozen	3	S3	2.04	32923	9877	13718	17.97	229
Morison and Sozen	4	S4	2.07	33200	9960	13833	16.51	215
Morison and Sozen	5	S5	2.08	33282	9985	13868	13.60	276
Hanson and Hanson	6	A12	2.02	32726	9818	13636	5.99	341
Hanson and Hanson	7	A13L	2	32613	9784	13589	6.02	330
Hanson and Hanson	8	B16	1.93	31919	9576	13300	7.18	381
Hanson and Hanson	9	C17	2.1	33500	10050	13958	7.37	336
Pan and Moehle	10	1	2.02	32754	9826	13648	28.06	267
Pan and Moehle	11	3	1.96	32212	9963	13422	39.20	269
Durani et al.	12	DNY1	2.08	33309	9993	13879	37.8	125
Durani et al.	13	DNY2	1.77	9143	135830	12698	31.8	105
Durani et al.	14	DNY3	1.74	9036	135830	12550	29.6	163
Durani et al.	15	DNY4	1.53	8461	135830	11752	24.6	179
Robertson and Durani	16	1	2.16	10210	135830	14181	40.00	162
Robertson and Durani	17	2C	2.01	9801	135830	13612	36.40	182
Robertson and Durani	18	3SE	2.32	10667	135830	14816	44.00	164
Robertson and Durani	19	4S	2.32	10660	135830	14806	43.80	169
Robertson and Durani	20	5SO	2.16	10210	135830	14181	40.00	167
Robertson and Durani	21	6LL	1.99	9733	135830	13518	12.15	211
Robertson and Durani	22	7L	1.94	9611	135830	13349	25.60	156
Robertson	23	8I	2.19	10312	125929	14323	37.80	176
Ghali at al.	24	SM0.5	2.12	10115	206184	14048	69.40	144
Ghali at al.	25	SM1.0	2.02	9835	206184	13659	64.80	198
Ghali at al.	26	SM1.5	2.21	10366	206184	14398	73.40	181
Farhey at al.	27	1	2.07	9976	73956	13856	17.20	192
Farhey at al.	28	2	2.07	9976	73956	13856	17.20	192
Farhey at al.	29	3	1.36	7976	73956	11078	4.64	409
Farhey at al.	30	4	1.36	7976	64404	11078	4.82	312

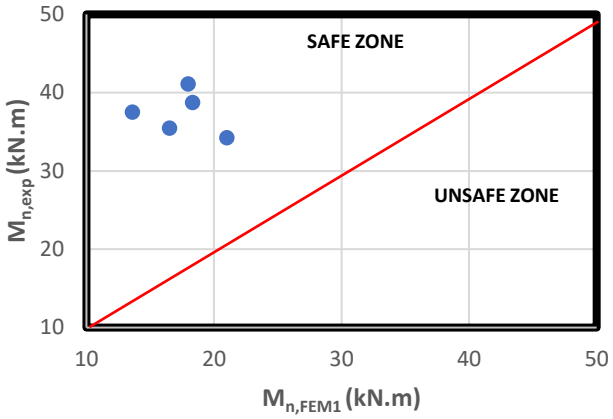

Figure 3.35 Comparison of Moment Capacity (Morison and Sozen, 1981)

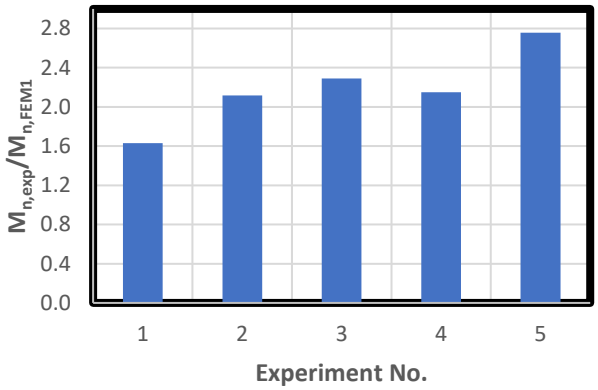

Figure 3.36 Moment Capacity Ratios, $M_{n,exp}/M_{n,FEM1}$ (Morison and Sozen, 1981)

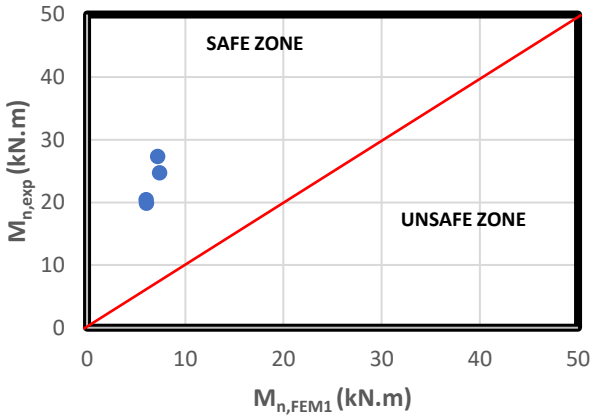

Figure 3.37 Comparison of Moment Capacity (Hanson and Hanson, 1968)

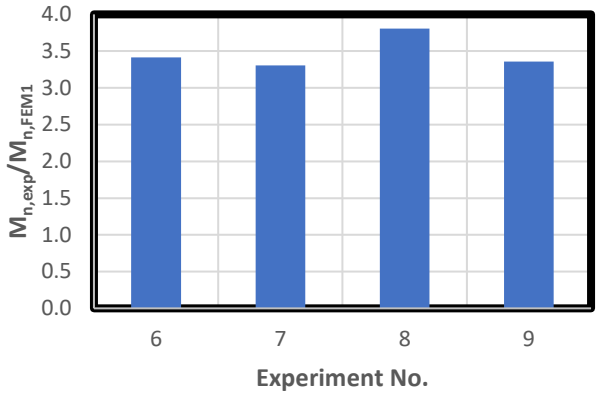

Figure 3.38 Moment Capacity Ratios, $M_{n,exp}/M_{n,FEM1}$ (Hanson and Hanson, 1968)

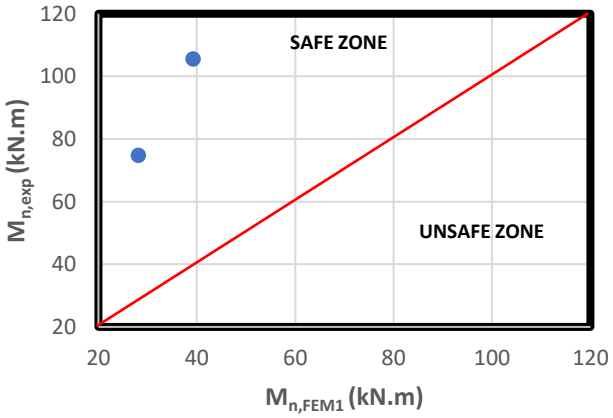

Figure 3.39 Comparison of Moment Capacity (Pan and Moehle, 1992)

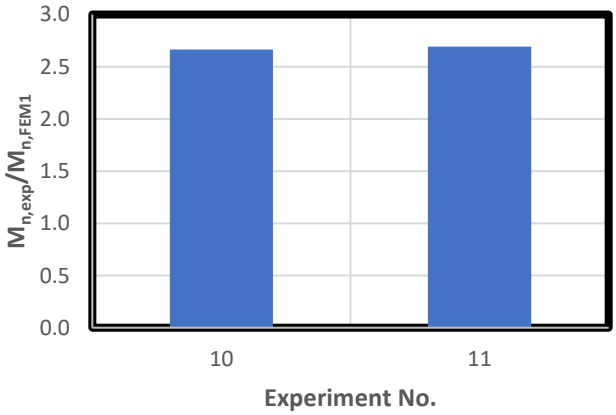

Figure 3.40 Moment Capacity Ratios, $M_{n,exp}/M_{n,FEM1}$ (Pan and Moehle, 1992)

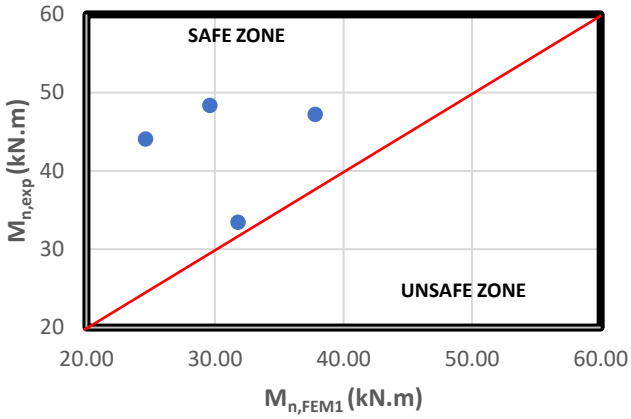

Figure 3.41 Comparison of Moment Capacity (Durani et al., 1995)

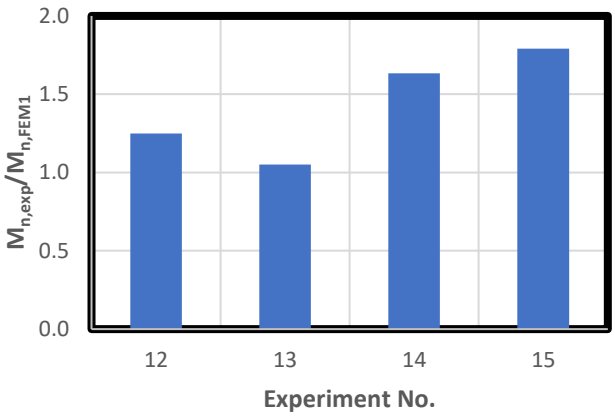

Figure 3.42 Moment Capacity Ratios, $M_{n,exp}/M_{n,FEM1}$ (Durani et al., 1995)

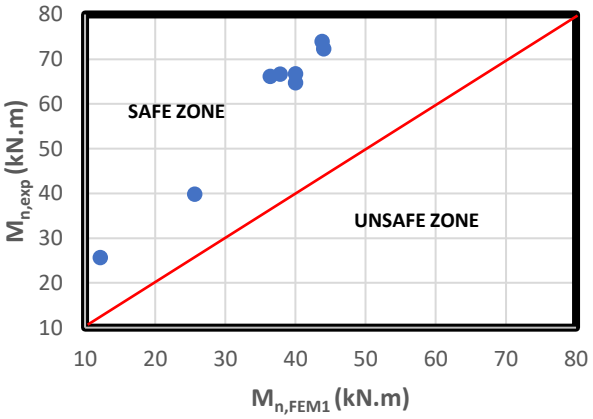

Figure 3.43 Comparison of Moment Capacity (Robertson and Durani, 1990)

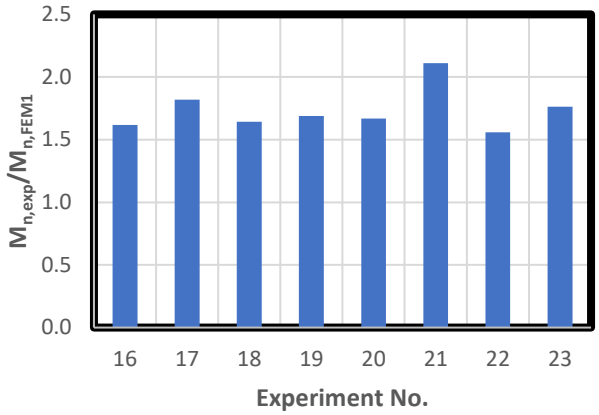

Figure 3.44 Moment Capacity Ratios, $M_{n,exp}/M_{n,FEM1}$ (Robertson and Durani, 1990)

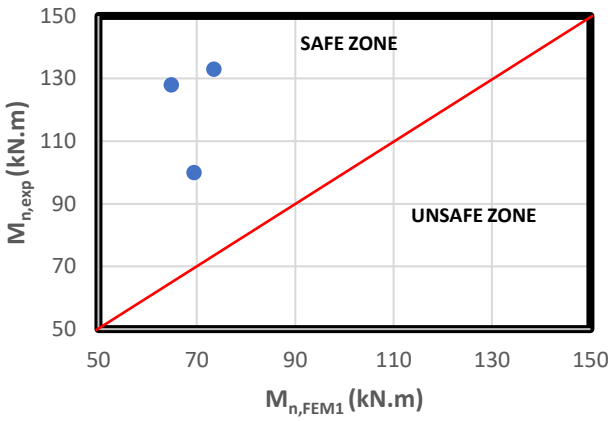

Figure 3.45 Comparison of Moment Capacity (Ghali et al., 1976)

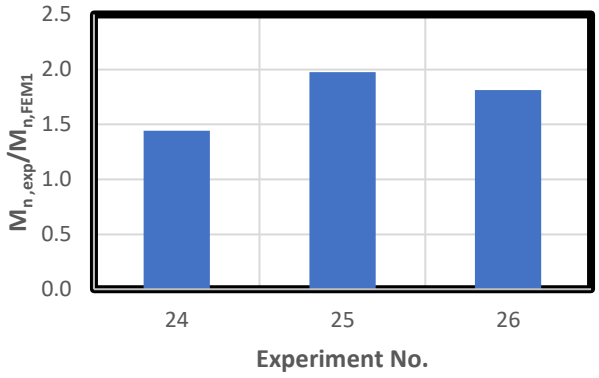

Figure 3.46 Moment Capacity Ratios, $M_{n,exp}/M_{n,FEM1}$ (Ghali et al., 1976)

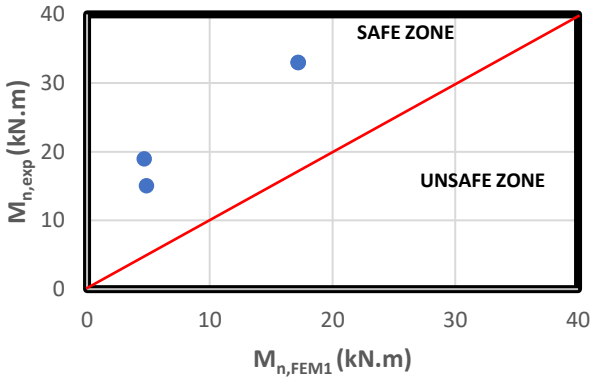

Figure 3.47 Comparison of Moment Capacity (Farhey et al., 1993)

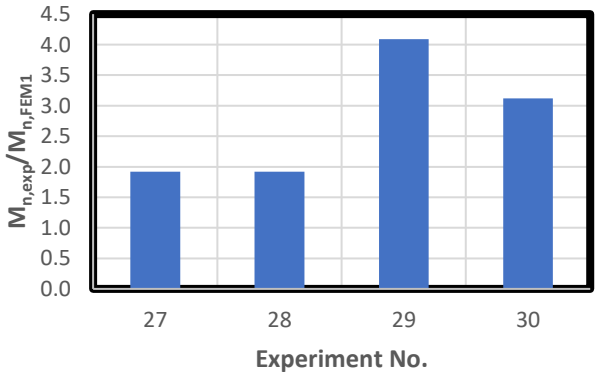

Figure 3.48 Moment Capacity Ratios, $M_{n,exp}/M_{n,FEM1}$ (Farhey et al., 1993)

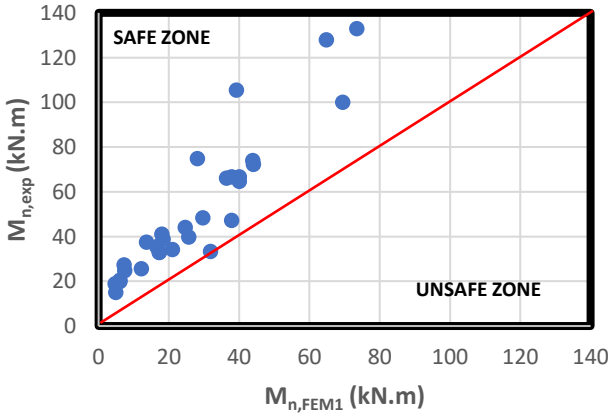

Figure 3.49 Comparison of Moment Capacity For the Group of Test Specimens Marked with A and AB

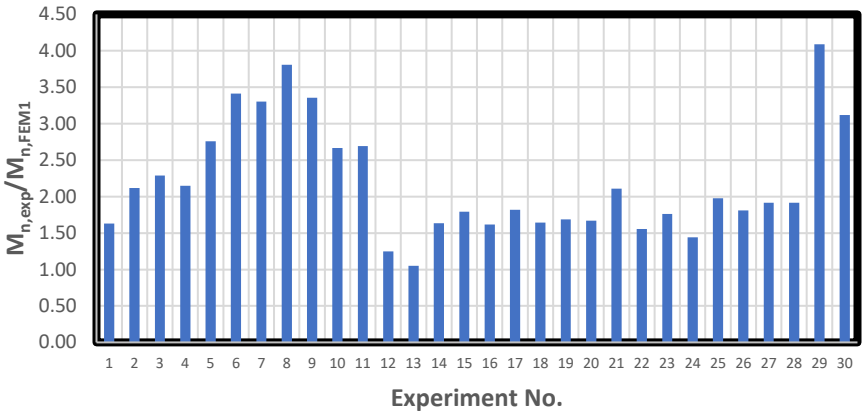

Figure 3.50 Moment Capacity Ratios, $M_{n,exp}/M_{n,FEM1}$ For the Group of Test Specimens Marked with A and AB

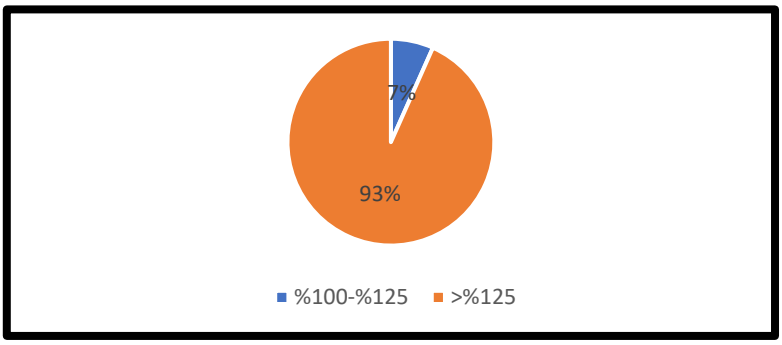

Figure 3.51 Distribution of $M_{n,exp}/M_{n,FEM1}$ Results

Table 3.5 Comparison of Experimental Results and FEM Results (For Approach 1)

Researcher	Average value of $M_{n,\,exp}/M_{n,\,FEM1}$ (%)	Standard Deviation of Results (%)
Morison and Sozen (1981)	219	36
Hanson and Hanson (1968)	347	20
Pan and Moehle (1992)	268	1
Durani et al. (1995)	143	29
Robertson and Durani (1990)	173	16
Ghali et al. (1776)	174	22
Farhey et al. (1993)	276	91
Average	220	77

3.3.2 Approach 2 (FEM2): Average Shear Stress Based Design

After analysis of 30 experimental slab-column connections included in the group of test specimens marked with A and AB, it is clearly seen that approach 2 gives better results compared to results obtained from approach 1. Generally, they were coincided with experimental results. Results are presented in Table 3.6 for Approach 2. Results are also shown in detail in Figures 52 to 65. Mean value of moment capacity ratios, $M_{n,exp}/M_{n,FEM2}$ and standart deviation of results are given in Table 3.7 for each set of data seperately. Mean value of moment capacity ratio, $M_{n,exp}/M_{n,FEM2}$ and standart deviations for thirty test specimen are also shown in Table 3.7. Based on the analysis results, mean value of moment capacity ratios, $M_{n,exp}/M_{n,FEM2}$ obtained from each set of data fluctuated between %84 and %155. Mean value is also equal to %114 with standart deviation %30 for thirty test specimen. Finite element model results obtained from approach 2 are very close the actual results of test specimen compared to results obtained from approach 1. In addtion, it can be stated that generally conservative results were obtained based on a mean value of moment capacity ratio ($M_{n,exp}/M_{n,FEM2}$) which is equal to %119. Even if each set of data compared with experimental results, all of them gave conservative results except that datasets of Morison and Sozen (1981) and Durani et al. (1995). Distribution of the moment capacity ratio,$M_{n,exp}/M_{n,FEM2}$, results in a specific range is also shown in Figure 3.70. As it is seen in Figure 3.70, only %10 finite element model gives highly unconservative results based on moment capacity ratio results, $M_{n,exp}/M_{n,FEM2}$ which are smaller than %75. %27 percent finite element model gives highly conservative results based on moment capacity ratio results, $M_{n,exp}/M_{n,FEM2}$ which are greater than %125. Remaning %63 finite element model gives approximately same results with experiments based on moment capacity ratio results between %75 and %125. Moreover, $M_{n,ESSM}/M_{n,FEM2}$ results are plotted in Figures 3.68 and 3.69. It is observed that finite element model results obtained by using approach 2 gives almost always conservative results considering $M_{n,ESSM}/M_{n,FEM2}$ is greater than %100.

Table 3.6 Finite Element Model Results for Approach 2

Researcher	Experiment No.	Specimen	$f_{ctd,TKDY}$, MPa	E_c, MPa	E_{cr}, MPa	G, mm^2	$M_{n,FEM2}$, kN.m	$M_{u,exp}/M_{n,FEM2}$ (%)
Morison and Sozen	1	S1	2.37	35995	10798	14998	51.60	66
Morison and Sozen	2	S2	2.07	33255	9976	13856	45.00	86
Morison and Sozen	3	S3	2.04	32923	9877	13718	44.20	93
Morison and Sozen	4	S4	2.07	33200	9960	13833	43.40	82
Morison and Sozen	5	S5	2.08	33282	9985	13868	41.00	91
Hanson and Hanson	6	A12	2.02	32726	9818	13636	11.90	172
Hanson and Hanson	7	A13L	2	32613	9784	13589	11.90	167
Hanson and Hanson	8	B16	1.93	31919	9576	13300	15.25	179
Hanson and Hanson	9	C17	2.1	33500	10050	13958	24.60	101
Pan and Moehle	10	1	2.02	32754	9826	13648	70.20	107
Pan and Moehle	11	3	1.96	32212	9963	13422	75.84	139
Durani et al.	12	DNY1	2.08	33309	9993	13879	56.20	84
Durani et al.	13	DNY2	1.77	9143	135830	12698	47.60	70
Durani et al.	14	DNY3	1.74	9036	135830	12550	44.80	108
Durani et al.	15	DNY4	1.53	8461	135830	11752	37.80	117
Robertson and Durani	16	1	2.16	10210	135830	14181	59.20	109
Robertson and Durani	17	2C	2.01	9801	135830	13612	54.40	122
Robertson and Durani	18	3SE	2.32	10667	135830	14816	64.80	112
Robertson and Durani	19	4S	2.32	10660	135830	14806	64.60	115
Robertson and Durani	20	5SO	2.16	10210	135830	14181	59.20	113
Robertson and Durani	21	6LL	1.99	9733	135830	13518	34.20	75
Robertson and Durani	22	7L	1.94	9611	135830	13349	42.20	95
Robertson	23	8I	2.19	10312	125929	14323	55.60	120
Ghali at al.	24	SM0.5	2.12	10115	206184	14048	97.40	103
Ghali at al.	25	SM1.0	2.02	9835	206184	13659	91.20	140
Ghali at al.	26	SM1.5	2.21	10366	206184	14398	102.80	129
Farhey at al.	27	1	2.07	9976	73956	13856	29.80	111
Farhey at al.	28	2	2.07	9976	73956	13856	29.80	111
Farhey at al.	29	3	1.36	7976	73956	11078	14.80	128
Farhey at al.	30	4	1.36	7976	64404	11078	8.07	186

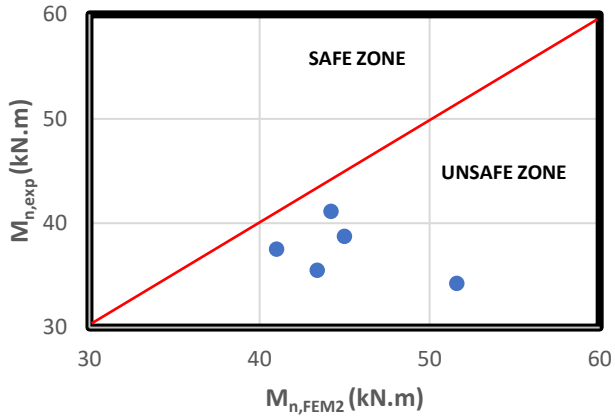

Figure 3.52 Comparison of Moment Capacity (Morison and Sozen, 1981)

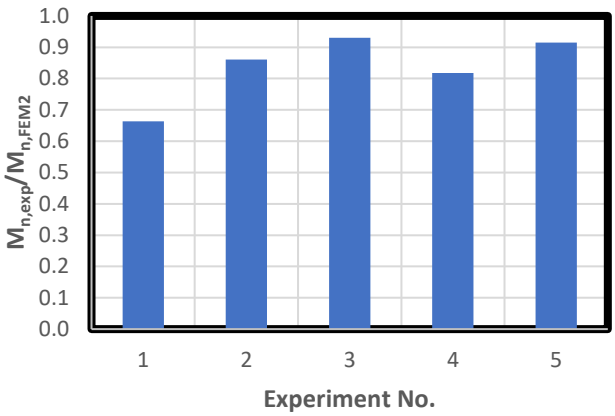

Figure 3.53 Moment Capacity Ratios, $M_{n,exp}/M_{n,FEM2}$ (Morison and Sozen, 1981)

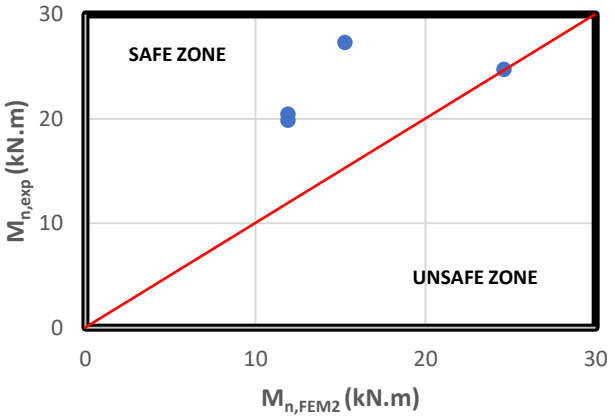

Figure 3.54 Comparison of Moment Capacity (Hanson and Hanson, 1968)

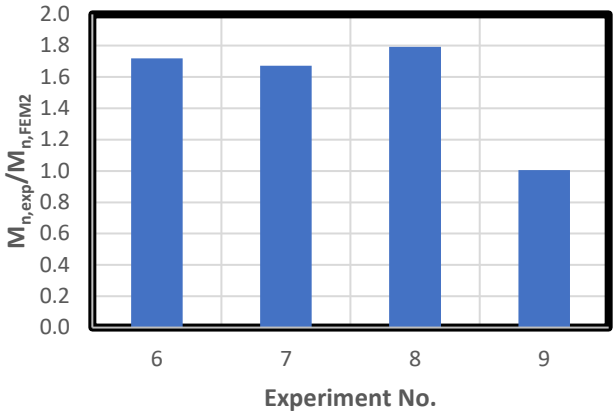

Figure 3.55 Moment Capacity Ratios, $M_{n,exp}/M_{n,FEM2}$ (Hanson and Hanson, 1968)

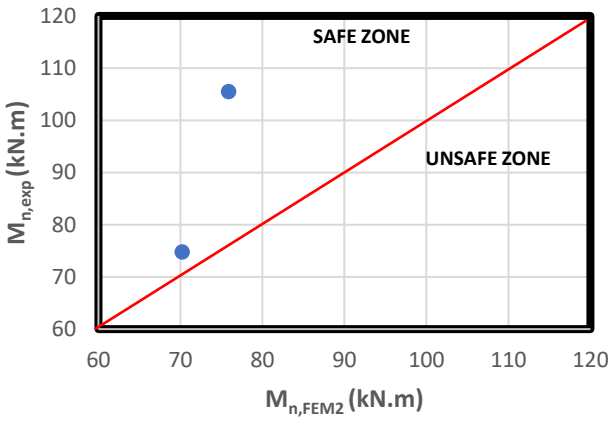

Figure 3.56 Comparison of Moment Capacity (Pan and Moehle, 1992)

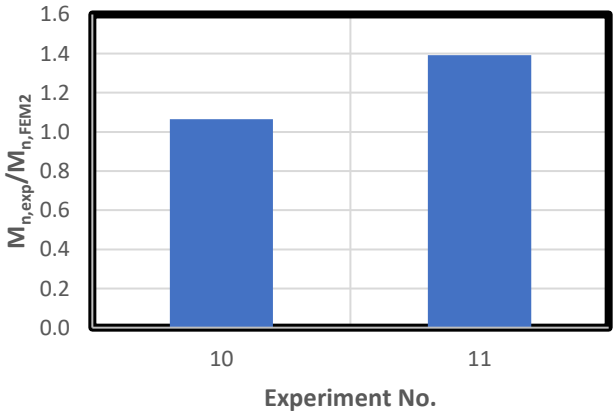

Figure 3.57 Moment Capacity Ratios, $M_{n,exp}/M_{n,FEM2}$ (Pan and Moehle, 1992)

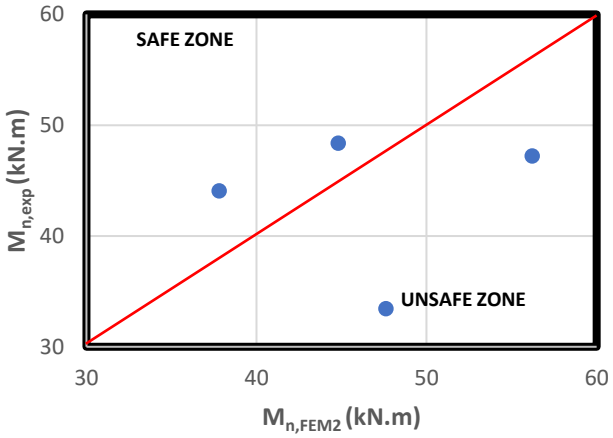

Figure 3.58 Comparison of Moment Capacity (Durani et al., 1995)

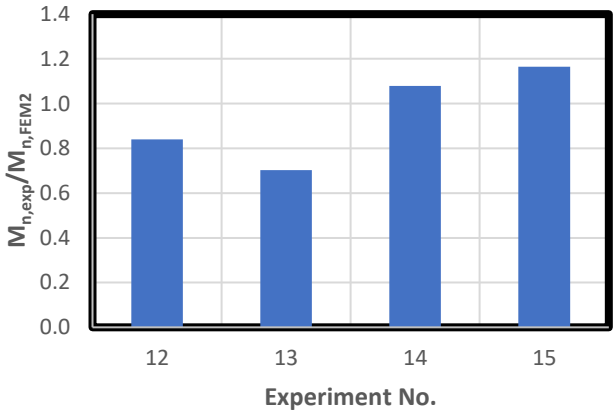

Figure 3.59 Moment Capacity Ratios, $M_{n,exp}/M_{n,FEM2}$ (Durani et al., 1995)

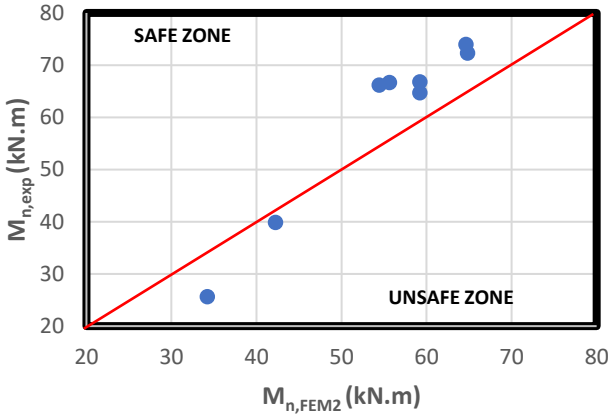

Figure 3.60 Comparison of Moment Capacity (Robertson and Durani, 1990)

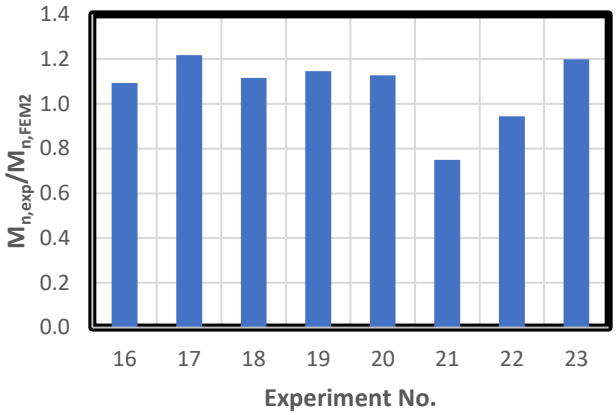

Figure 3.61 Moment Capacity Ratios, $M_{n,exp}/M_{n,FEM2}$ (Robertson and Durani, 1990)

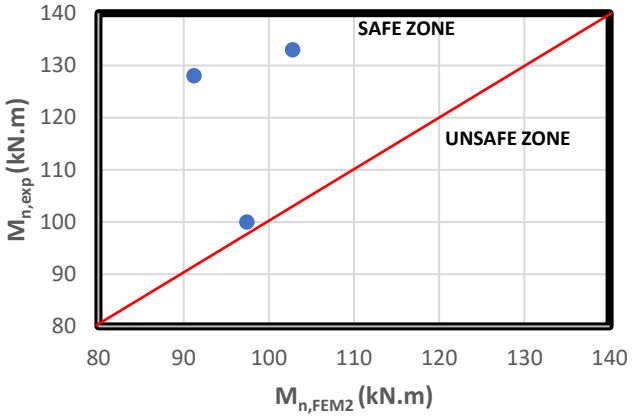

Figure 3.62 Comparison of Moment Capacity (Ghali et al., 1976)

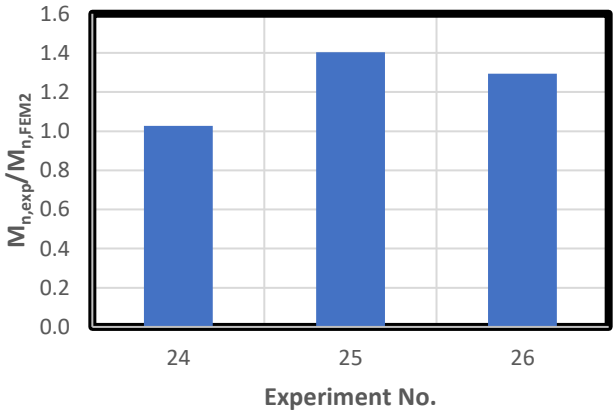

Figure 3.63 Moment Capacity Ratios, $M_{n,exp}/M_{n,FEM2}$ (Ghali et al., 1976)

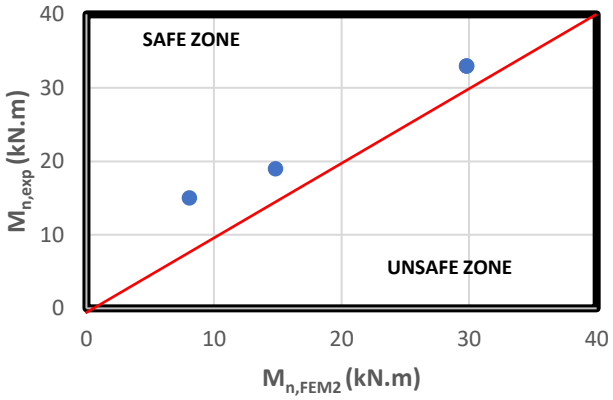

Figure 3.64 Comparison of Moment Capacity (Farhey et al., 1993)

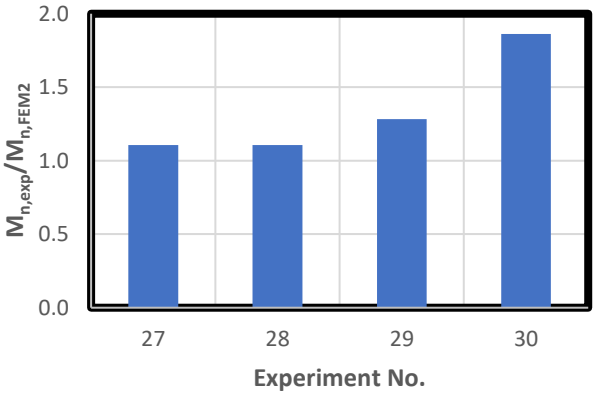

Figure 3.65 Moment Capacity Ratios, $M_{n,exp}/M_{n,FEM2}$ (Farhey et al., 1993)

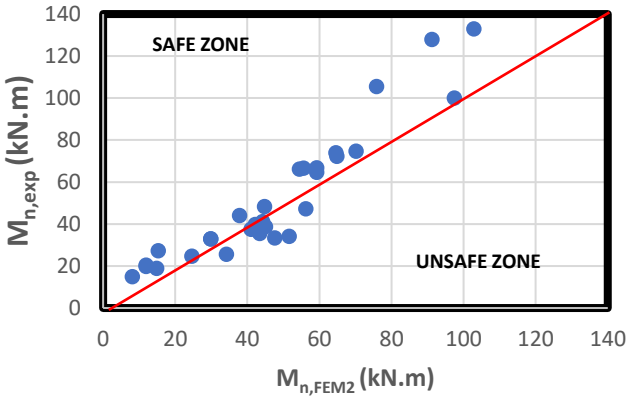

Figure 3.66 Comparison of Moment Capacity for the Group of Test Specimens Marked with A and AB

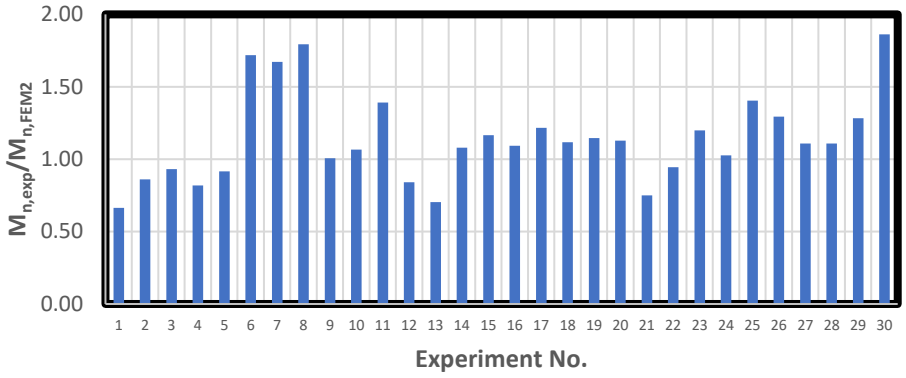

Figure 3.67 Moment Capacity Ratios, $M_{n,exp}/M_{n,FEM2}$ For the Group of Test Specimens Marked with A and AB

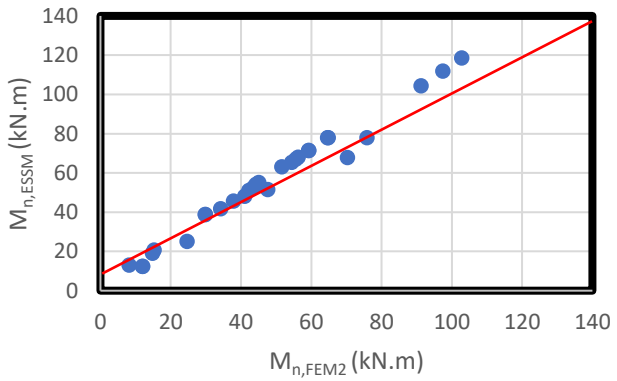

Figure 3.68 Comparison of Moment Capacity for the Group of Test Specimens Marked with A and AB

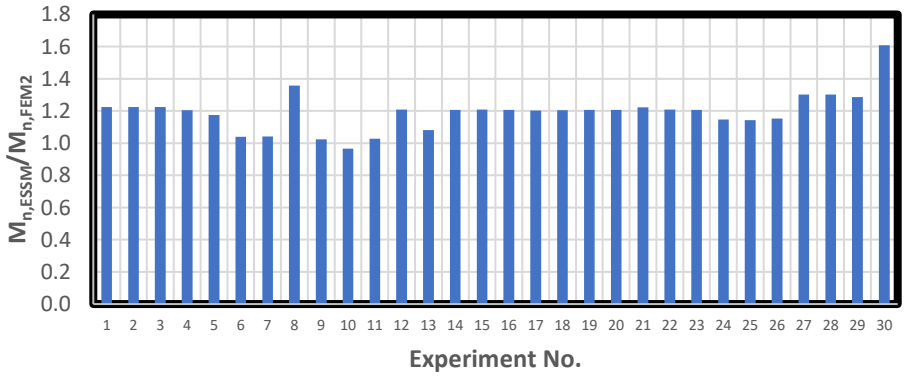

Figure 3.69 Moment Capacity Ratios, $M_{n,ESSM}/M_{n,FEM2}$ For the Group of Test Specimens Marked with A and AB

Table 3.7 Comparison of Experimental Results and FEM Results For Approach 2

Researcher	Average value of $M_{n,\,exp}/M_{n,\,FEM2}$ (%)	Standard Deviation of Results (%)
Morison and Sozen (1981)	84	10
Hanson and Hanson (1968)	155	32
Pan and Moehle (1992)	123	16
Durani et al. (1995)	95	18
Robertson and Durani (1990)	107	14
Ghali et al. (1976)	124	16
Farhey et al. (1993)	134	31
Average	114	30

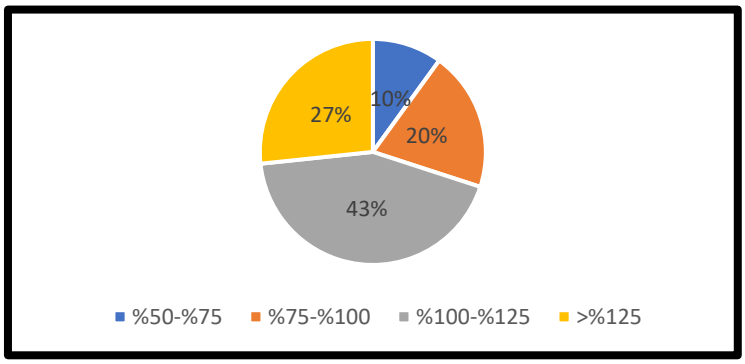

Figure 3.70 Distribution of $M_{n,exp}/M_{n,FEM2}$ Results

3.3.3 Mesh Size Effects on Finite Element Model Results

In the previous part, finite element models created with mesh size equal to half of effective slab depth, d/2. Using mesh size greater than d/2 is not proper to define perimeter line correctly because it should be far away from the column face as a distance d/2. Even if it is used only for shell elements outside and inside of perimeter and bigger mesh size is used for remaining part of the shell elements, taking average shear stress on the perimeter line at critical side by using approach 2 cannot give good results due to huge differences between mesh sizes. At this time, mesh width also should be considered, and average shear stress shouldn't be found directly

without not considering difference on mesh size. Finite element models which have finer, and equal mesh also give better results. So, shell elements used for modelling of slab should be meshed finer and equal as far as column dimensions allow. Half of effective slab depth, d/2 can be recommended as a maximum mesh size. If designer wants to model slab with finer mesh, mesh size also should be multiplier of d/2.

In this part, mesh size effects on moment capacity of the connection are examined. Some of the test specimen modelled with finer mesh size of d/4. Mesh size of d/2 used for finite element models analyzed in previous part varies in a wide range between 28.6 mm and 60.5 mm. In the literature, recommended value for minimum mesh size should be greater than the aggregate size. If it is assumed that aggregate size equal to approximately 20 mm, minimum mesh size should be higher than this value. Therefore, test specimen which have effective slab depth four time greater than aggregate size were modelled with mesh size d/4. Experiments number differs from 10 to 26 totally 17 test specimens were modelled with mesh size of d/4.

It is exact that moment capacity estimations of the connection modelled with finer mesh decreases using approach 1. As it is shown in Figure 3.28 and Figure 3.29, shear stress increases towards the corner of the column. If mesh size is finer, shell element at corner of the column gives higher shear stress for local finer mesh area under same loading. This means that, lateral force should be decreased to obtain critical shear stress on the perimeter. Naturally, moment capacity of the connection decreases by decreasing of lateral force. As it is stated before, moment capacities obtained from finite element models using approach 1 gives very conservative results. If finer mesh is used for approach 1, results will be more conservative. Therefore, mesh study is not further sought for approach 1.

Moment capacity of the connection obtained from finite element models which have mesh size of d/4 for approach 2 is shown in Table 3.8. Moment capacity of the connection increases approximately %9 by using finer mesh size of d/4.

Finite element model results using approach 2 with mesh size arranged approximately between 2cm and 3cm were compared with experimental results in

Table 3.9. Mean of $M_{n,exp}/M_{n,FEM2}$ for thirty test specimen is equal to %109 with standard deviation %31.

Table 3.8 Mesh Size Effects

Researcher	Experiment No.	Specimen	Mesh Size in terms of d	Mesh Size, mm	$M_{n,FEM2}$, kN.m (Mesh size, d/4)	$M_{n,FEM2}$, kN.m (Mesh size,d/2)	$M_{n,FEM2(d/4)}/M_{n,FEM2(d/2)}$
Morison and Sozen	1	S1	d/2	30.5	-	51.60	-
Morison and Sozen	2	S2	d/2	30.5	-	45.00	-
Morison and Sozen	3	S3	d/2	30.5	-	44.20	-
Morison and Sozen	4	S4	d/2	30.5	-	43.40	-
Morison and Sozen	5	S5	d/2	30.5	-	41.00	-
Hanson and Hanson	6	A12	d/2	28.6	-	11.90	-
Hanson and Hanson	7	A13L	d/2	28.6	-	11.90	-
Hanson and Hanson	8	B16	d/2	28.6	-	15.25	-
Hanson and Hanson	9	C17	d/2	28.6	-	24.60	-
Pan and Moehle	10	1	d/4	25.85	76.60	70.20	109
Pan and Moehle	11	3	d/4	25.85	81.66	75.84	108
Durani et al.	12	DNY1	d/4	24.2	60.12	56.20	107
Durani et al.	13	DNY2	d/4	24.2	51.80	47.60	109
Durani et al.	14	DNY3	d/4	24.2	48.80	44.80	109
Durani et al.	15	DNY4	d/4	24.2	41.40	37.80	110
Robertson and Durani	16	1	d/4	24.2	64.40	59.20	109
Robertson and Durani	17	2C	d/4	24.2	59.00	54.40	108
Robertson and Durani	18	3SE	d/4	24.2	70.20	64.80	108
Robertson and Durani	19	4S	d/4	24.2	70.20	64.60	109
Robertson and Durani	20	5SO	d/4	24.2	64.40	59.20	109
Robertson and Durani	21	6LL	d/4	24.2	38.80	34.20	113
Robertson and Durani	22	7L	d/4	24.2	46.60	42.20	110
Robertson	23	8I	d/4	22.8	60.20	55.60	108
Ghali at al.	24	SM0.5	d/4	30.25	104.20	97.40	107
Ghali at al.	25	SM1.0	d/4	30.25	97.80	91.20	107
Ghali at al.	26	SM1.5	d/4	30.25	110.00	102.80	107
Farhey at al.	27	1	d/2	29.85	-	29.80	-
Farhey at al.	28	2	d/2	29.85	-	29.80	-
Farhey at al.	29	3	d/2	29.85	-	14.80	-
Farhey at al.	30	4	d/2	29.85	-	8.07	-

Table 3.9 Comparison of Experimental Results and FEM Results For Approach 2 with Mesh Size between 2cm and 3cm

Researcher	Mesh Size in terms of d	Average value of $M_{n,\,exp}/M_{n,\,FEM2}$ (%)	Standard Deviation of Results (%)
Morison and Sozen (1981)	d/2	84	10
Hanson and Hanson (1968)	d/2	155	32
Pan and Moehle (1992)	d/4	113	16
Durani et al. (1995)	d/4	87	17
Robertson and Durani (1990)	d/4	98	14
Ghali et al. (1776)	d/4	116	15
Farhey et al. (1993)	d/2	134	31
Average		109	31

Table 3.10 Mesh Convergence Study

Researcher	**Specimen**	**Mesh Size, in d**	**Lateral Force (kN)**	**Lateral Drift, Δ (mm)**	**Difference in Drift (%)**	**Max, Shear, FEM1, MPa**	**Difference in Shear (%)**	**Avg, Shear, FEM2, MPa**	**Difference in Shear (%)**
Morison and Sozen	S1	d/2	10	2.63	-	1.30	-	0.54	-
	S1	d/4	10	2.66	1.14	1.35	3.95	0.50	6.11
	S1	d/8	10	2.67	0.38	1.34	0.96	0.50	1.56
Hanson and Hanson	A12	d/2	2.5	3.13	-	1.60	-	0.98	-
	A12	d/4	2.5	3.16	0.96	1.70	5.88	0.93	5.41
	A12	d/8	2.5	3.17	0.32	1.73	1.74	0.92	1.19
Pan and Moehle	1	d/2	10	3.48	-	1.76	-	0.86	-
	1	d/4	10	3.54	1.72	1.94	10.20	0.79	7.98
	1	d/8	10	3.55	0.28	1.90	1.60	0.78	1.83

Mesh size smaller than d/4 can also be used for modelling slab of actual buildings by providing minimum aggregate size because slab thickness of actual buildings is high compared to the one of test specimens. Even if mesh size which is smaller than

minimum aggregate size is not considered as efficient in modelling, it was also studied in which mesh size the results converged. Three different test specimens were evaluated in this scope. The results of these test specimens are shown in Table 3.10. It is obvious that results are converged with mesh size d/4 and all results of finite element models which have mesh size d/4 and d/8 are almost similar each other.

3.3.4 Results for Biaxial Lateral Load

Most of the experiment in the literature were conducted under uniaxial lateral load. A small number of researchers conducted experiment to observe effects of biaxial lateral loading. Hwang and Moehle, 1989 tested nine panel flat plate frame under biaxial load. In addition, Pan and Moehle, 1992 investigated behavior of slab column connection under uniaxial load as well as biaxial load. In this experiment, four test specimens were included, all of them consist of single slab-column connections and two of them were tested under biaxial lateral load.

Second test specimen of Pan and Moehle, 1992 were modelled. All parameters and properties of second test specimen is similar with first test specimen which is shown in Table 3.1. Unlike the uniaxial lateral loading, each side of the slab were restricted with roller supports assuming edges are contraflexure point of slab and lateral loads were applied at the top of column in two lateral directions. For each load level, maximum shear stress and average shear stress were calculated. These results were also compared with eccentric shear stress model results. While calculating shear stress for eccentric shear stress model, unbalanced moments occurred in two directions on the connections in the finite element model were used. The general view of finite element model is shown in Figure 3.71.

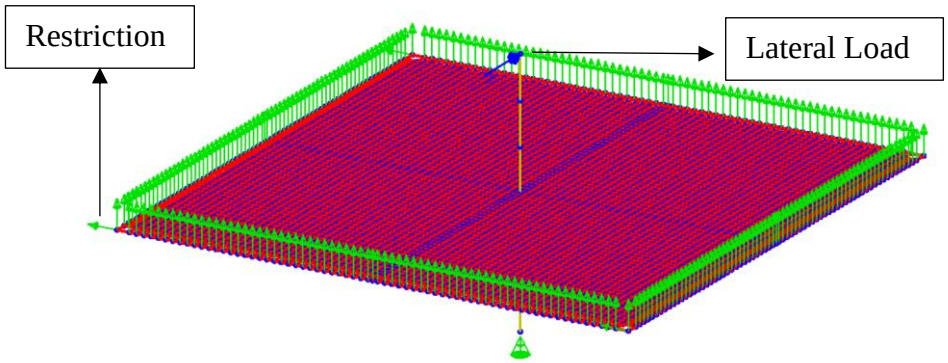

Figure 3.71 General View of FEM (Step 3)

Construction stage analysis was used to analyze the model. In the first step, test specimen was constructed, and self-weight of the system was defined. In second step, superimposed dead load was applied. At the end of second step, amount of gravity force measured in experiment and calculated in LARSA 4D were equalized. Then, lateral forces which is in each lateral direction were applied in third and fourth step. There is a reminder here. As it is seen from Figure 3.71, edge joints of the slab were also restricted in direction perpendicular to loading direction to prevent obtaining unstable results.

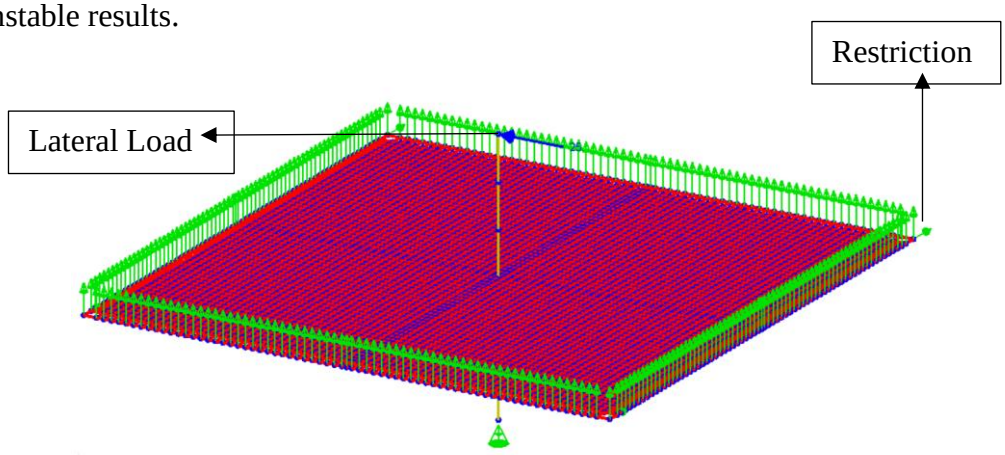

Figure 3.72 General View of FEM (Step 4)

In the next step, lateral load was applied in other direction. The joint restriction should provide stability of system. Therefore, the restriction of edge joints was changed by using support ?? Hoist activities in step 4. Joint restriction changed in step 4 is shown in Figure 3.72.

Shear stress distribution obtained from the analysis results are shown in Figures 3.73 and 3.74. In the scope of approach 1, maximum shear stress occurred at shell 3 and 6 were taken as a critical shear stress. However, in the scope approach 2, avarage shear stress of shell elements from number 1 to 4 or 5 to 8 were taken as a critical shear stress.

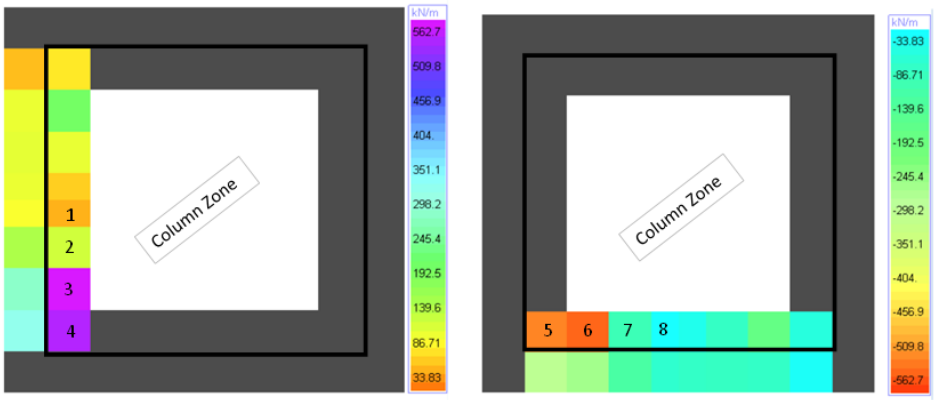

Figure 3.73 Critical Shear Stress on Punching Perimeter

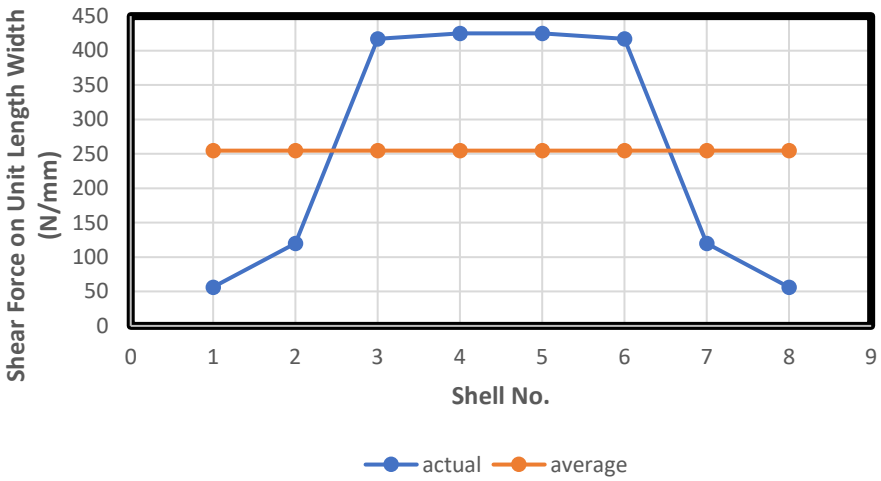

Figure 3.74 Actual and Average Shear Stress Distribution on Critical Punching Perimeter Line

Critical shear stress was calculated with Equation 3.5 for eccentric shear stress model in TBDY 2018.

$$v_c = \frac{V_u}{A_c} \pm \frac{\gamma_v \times M_{ux} \times c_x}{J_{cx}} \pm \frac{\gamma_v \times M_{uy} \times c_y}{J_{cy}} \quad (3.5)$$

Results are presented in Table 3.11.

Table 3.11 Comparison of ESSM and FEM Results for Connection Biaxially Loaded

LATERAL FORCE, Fx-Fy (kN)	Max. Shear Stress (MPa) Approach 1	Avg. Shear Stress (MPa) Approach 2	Mx (kN.m)	My (kN.m)	V (kN)	Shear Stress for ESSM (MPa)
5-5	1.67	1.00	9.15	9.15	103.5	1.03
5-10	1.95	1.20	9.15	18.3	103.5	1.21
10-10	2.28	1.36	18.3	18.3	103.5	1.39
10-15	2.56	1.57	18.3	27.45	103.5	1.58
15-15	2.89	1.73	27.45	27.45	103.5	1.76
15-20	3.16	1.93	27.45	36.6	103.5	1.94
20-20	3.50	2.1	36.6	36.6	103.5	2.11
25-20	3.77	2.30	36.6	45.76	103.5	2.31
25-25	4.11	2.46	45.76	45.76	103.5	2.49

It is clearly seen that maximum shear stress-based design (approach 1) gives conservative results compared to eccentric shear stress model results. However, average shear stress-based design (approach 2) gives similar results with eccentric shear stress model.

3.4 Improvement of Eccentric Shear Stress Model

In this section, an attempt was made to improve the eccentric shear stress model. Contribution factor of transferred moment carried by shear capacity of slab is formulated with Equation 1.1 and Equation 1.5 in the original eccentric shear stress model. It is clearly seen that contribution factor of transferred moment carried by flexural and shear capacity of slab only depends on column aspect ratio in the original model. However, experimental studies show that there are also two important parameter affects the contribution factor of transferred moment. One of them is gravity shear ratio and the other one is flexural reinforcement ratio. $M_{n,exp}/M_{n,ESSM}$ vs Flexural reinforcement ratio graph are shown in Figure 3.75. It is obvious that moment capacity ratio increases by increasing of flexural reinforcement ratio. This means that while eccentric shear stress model overestimates moment capacity of the connection for low flexural reinforcement ratio, it underestimates moment capacity of the connection for high flexural reinforcement ratio.

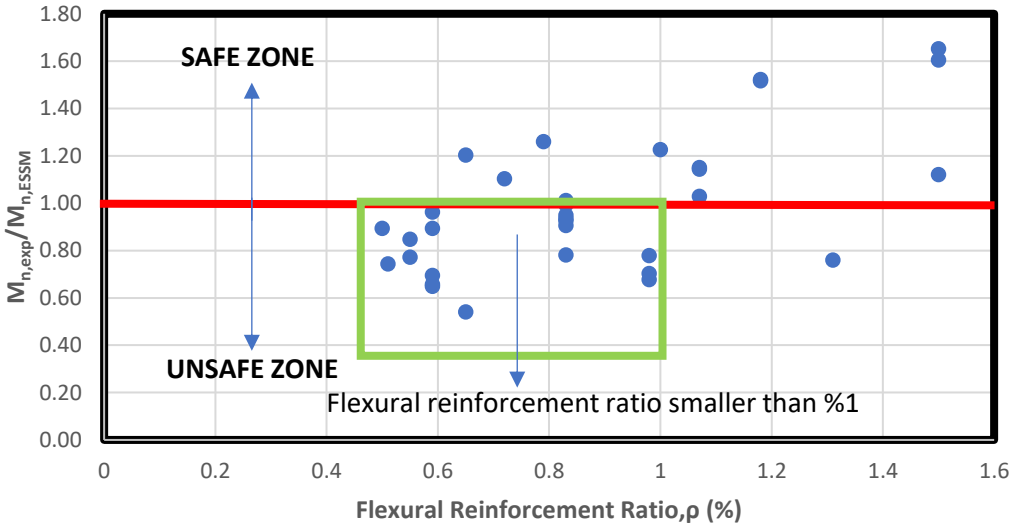

Figure 3.75 Effects of Flexural Reinforcement Ratio on Estimation of Moment Capacity by Using Eccentric Shear Stress Model for Test Specimen Marked with AB and B

It is also seen that eccentric shear stress model gives unsafe results for most of the test specimen with flexural reinforcement ratio smaller than %1. If it is considered that generally slabs are designed with flexural reinforcement ratio smaller than %1, finding of unsafe results by using eccentric shear stress model is probable.

Luo and Durani (1995) derived a formula to estimate contribution factor of transferred moment carried by shear capacity of slab,γ_v. Formula is shown in Equation 2.1. Contribution factor, γ_v depends on two parameters according to this formula. One of them is column aspect ratio and the other one is flexural reinforcement ratio. Effects of gravity shear ratio on contribution factor is ignored and it is said that formula is derived from results of test specimens which have gravity shear ratio higher than 0.15. Even if it is well known that high gravity shear ratio decreases moment capacity of the connection, it is not exactly known effects of gravity shear ratio on contribution of transferred moment carried by shear.

Moment capacity ratio vs gravity shear ratio graph is shown in Figure 3.76. It is not exactly possible to say that using of eccentric shear stress model gives safe results in a specific range of gravity shear ratio between 0 and 0.5. However, it is observed that there is correlation between gravity shear ratio and moment capacity ratio. In other words, eccentric shear stress model tends to underestimate moment capacity of the connection by increasing of gravity shear ratio.

In this section, new equation was derived to estimate contribution factor, γ_v considering effects of flexural reinforcement and gravity shear ratio. Most of the test specimen included in database constructed with square columns. Total number of test specimens which have square and rectangular column is 34 and 6, respectively. Therefore, only test specimens marked with AB and B constructed with square column were used to derive the contribution factor formula ignoring effects of column aspect ratio. There is an important reminder at this point. Despite test specimen 11 and test specimen 21 were constructed with square column, they were not included in the group of test specimens marked AB and B due to their misrepresentative results.

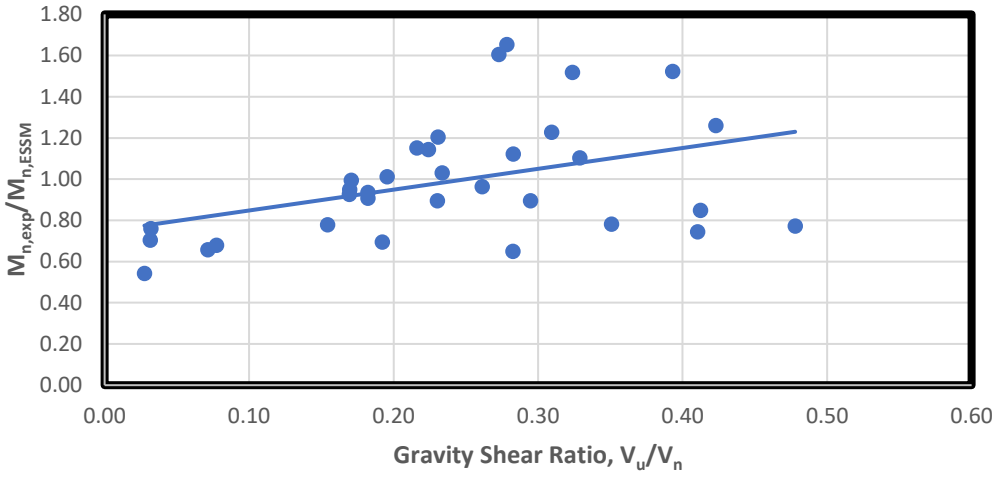

Figure 3.76 Effects of Gravity Shear Ratio on Estimation of Moment Capacity by Using Eccentric Shear Stress Model for Test Specimen Marked with AB and B

Contribution factor, $\gamma_{v,exp}$ was back calculated by using the experimental results into the Equation 3.6 derived from Equation 1.6.

$$\gamma_{v,exp} = \frac{\left(v_c - \frac{V_u}{A_c}\right) \times J_c}{M_u \times c} \tag{3.6}$$

Afterwards, calculated $\gamma_{v,exp}$ values were plotted depending on flexural reinforcement ratio and new γ_v equation was derived depending on flexural reinforcement ratio including effect of gravity shear ratio. $\gamma_{v,exp}$ results which was back calculated are shown in Figure 3.77 and 3.78. Equation was derived to estimate contribution factor, γ_v is shown in Equation 3.7.

$$\gamma_{v,estimated} = 0.78 - 25\rho - 0.54\frac{V_u}{V_n} \tag{3.7}$$

Contribution factor for the group of test specimens marked with AB and B were recalculated using formula in Equation 3.7. Then moment capacities of test specimen calculated again by using formula which is shown in Equation 3.2. Contribution factors,γ_v, moment capacities and moment capacity ratios for eccentric shear stress model, improved eccentric shear stress model, eccentric shear stress model improved by Luo and Durani (1995) and eccentric shear stress model in Eurocode are given in

Table 3.12. Mean and standard deviation of moment capacity ratios are also shown in Table 3.12.

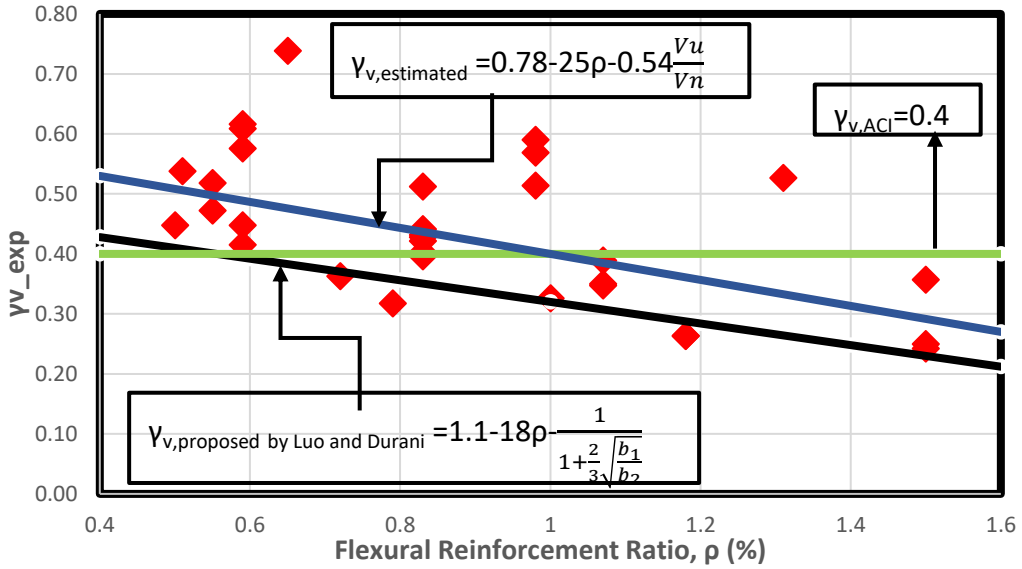

Figure 3.77 Estimation of Contribution Factor, γ_v Based on Flexural Reinforcement Ratio

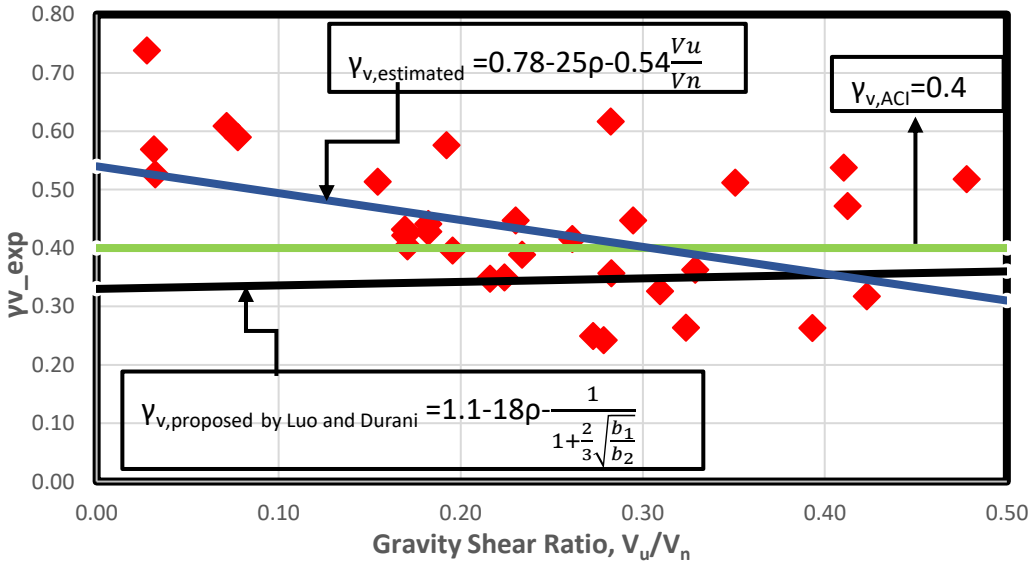

Figure 3.78 Estimation of Contribution Factor, γ_v Based on Gravity Shear Ratio

In the group of test specimens marked with AB and B, mean of moment capacity ratios are %98, %100, %81 and %102 for eccentric shear stress model, improved eccentric shear stress model, eccentric shear stress model improved by Luo and

Durani (1995), and eccentric shear stress model in Eurocode, respectively. Standard deviations are also %28, %15, %17, %18 respectively. These results show that even if eccentric shear stress model and improved eccentric shear stress model give similar results as a mean in terms of moment capacity ratio, improved model is better than the original model by estimating actual moment capacities of connection with a lower standard deviation. In addition, eccentric shear stress model in Eurocode gives good results compared to original eccentric shear stress model but improved model predicts moment capacity of the connection slightly better than eccentric shear stress model in Eurocode. Measured moment capacity in experiment vs predicted moment capacity for each eccentric shear stress model graphs were presented in Figures 3.79 to 3.82. Ratio of measured moment capacity to predicted moment capacity for different gravity ratios were also presented in Figures 3.83 to 3.87. Distribution of $M_{n,exp}/M_{n,ESSM\_estimated}$ results in a specific range was also shown in Figure 3.88. It is clearly seen that, %90 of moment capacity ratio results is between %75 and %125 and this shows that improved model predicts moment capacities of connection very close to moment capacity measured in experiments. Model improved by Luo and Durani doesn't estimate moment capacity of the connection very well. The main reason of worse estimation is probably using different dataset while deriving contribution factor,γ_v equation because researcher said that this contribution factor equation is derived depending on test results obtained for test specimens have only punching failure mode. (Luo and Durani, 1995)

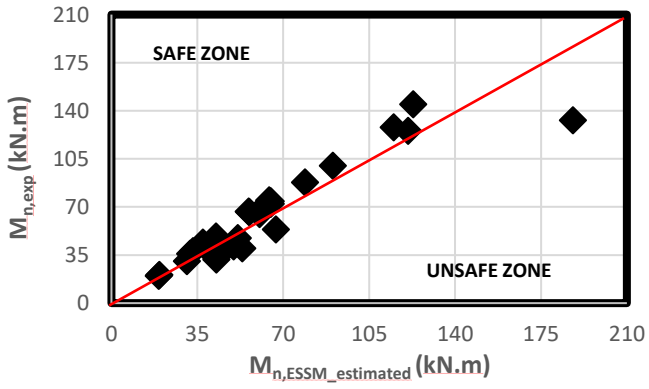

Figure 3.79 Comparison of Moment Capacity for the Group of Test Specimens Marked with AB and B (Improved Eccentric Shear Stress Model)

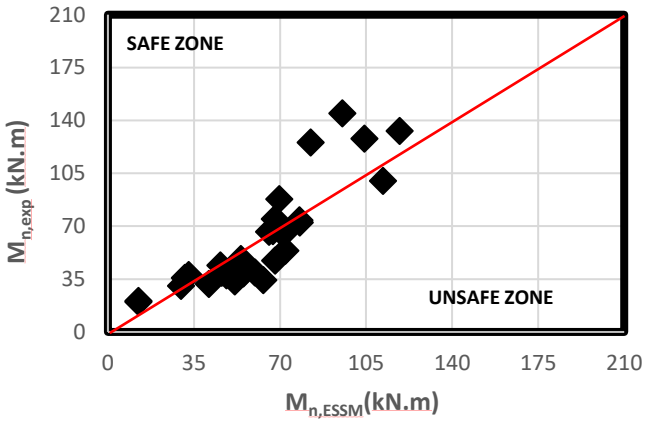

Figure 3.80 Comparison of Moment Capacity for the Group of Test Specimens Marked with AB and B (Original Eccentric Shear Stress Model)

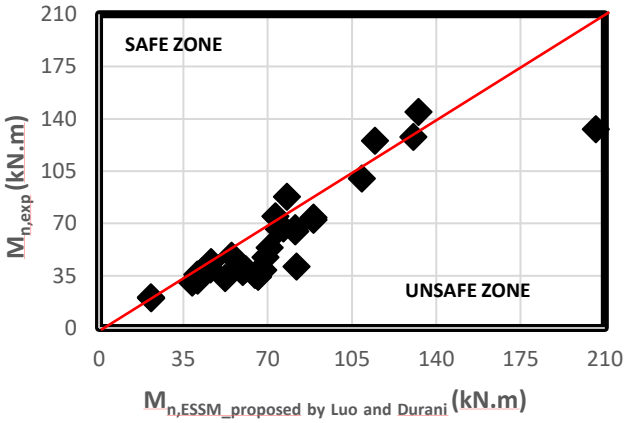

Figure 3.81 Comparison of Moment Capacity for the Group of Test Specimens Marked with AB and B (Proposed by Luo and Durani, 1995)

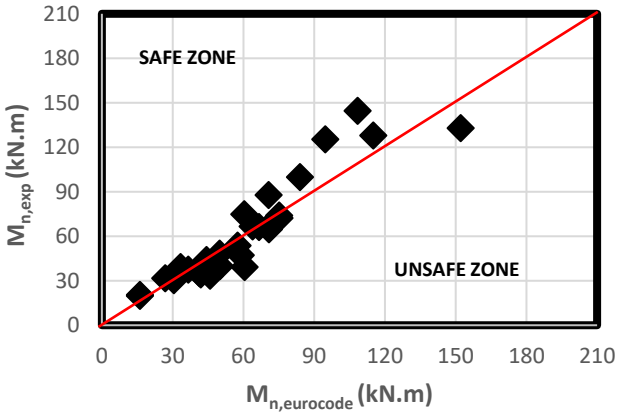

Figure 3.82 Comparison of Moment Capacity for the Group of Test Specimens Marked with AB and B (Eccentric Shear Stress Model in Eurocode 2)

Table 3.12 Improved Eccentric Shear Stress Model Results

Researcher	Experiment No	Specimen	$\gamma_{v,ESSM}$	$\gamma_{v,estimated}$	γ_v, (Luo and Durani)	$M_{n,ESSM}$	$M_{n,ESSM,estimated}$	$M_{n,ESSM,}$ (Luo and Durani)	$M_{n,eurocode}$	$M_{n,exp}/M_{n,ESSM}$ (%)	$M_{n,exp}/M_{n,ESSM,estimated}$ (%)	$M_{n,exp}/M_{n,ESSM}$ (%)(Luo and Durani)	$M_{n,exp}/M_{n,eurocode}$ (%)
Morison and Sozen	1	S1	0.4	0.60	0.38	63.17	41.93	65.98	41.88	54	82	52	82
Morison and Sozen	2	S2	0.4	0.52	0.32	55.08	42.53	68.09	44.01	70	91	57	88
Morison and Sozen	3	S3	0.4	0.44	0.26	54.10	49.71	81.91	48.05	76	83	50	86
Morison and Sozen	4	S4	0.4	0.49	0.32	52.32	42.43	64.67	41.15	68	84	55	86
Morison and Sozen	5	S5	0.4	0.45	0.32	48.17	42.65	59.54	36.60	78	88	63	102
Hanson and Hanson	6	A12	0.4	0.25	0.23	12.37	19.43	21.51	16.03	165	105	95	128
Hanson and Hanson	7	A13L	0.4	0.26	0.23	12.39	19.23	21.55	16.10	160	103	92	124
Pan and Moehle	10	1	0.4	0.42	0.37	67.80	64.20	73.22	60.32	110	117	102	124
Durani et al.	12	DNY1	0.4	0.53	0.39	67.98	51.42	69.05	58.78	69	92	68	80
Durani et al.	13	DNY2	0.4	0.48	0.39	51.52	42.93	52.33	45.78	65	78	64	73
Durani et al.	14	DNY3	0.4	0.51	0.39	54.08	42.56	54.93	49.90	89	114	88	97
Durani et al.	15	DNY4	0.4	0.49	0.39	45.73	37.22	46.45	44.28	96	118	95	99
Robertson and Durani	16	1	0.4	0.47	0.35	71.40	60.24	81.46	70.71	91	107	79	92
Robertson and Durani	17	2C	0.4	0.47	0.35	65.45	56.07	74.68	66.59	101	118	89	99
Robertson and Durani	18	3SE	0.4	0.48	0.35	78.04	64.89	89.04	75.20	93	111	81	96
Robertson and Durani	19	4S	0.4	0.48	0.35	77.93	64.81	88.91	75.13	95	114	83	98
Robertson and Durani	20	5SO	0.4	0.43	0.35	71.40	60.24	81.46	70.71	94	111	82	94
Robertson and Durani	22	7L	0.4	0.38	0.35	51.04	53.28	58.23	50.04	78	75	68	80
Robertson	23	8I	0.4	0.48	0.35	67.07	55.85	76.52	63.88	99	119	87	104
Ghali at al.	24	SM0.5	0.4	0.50	0.41	111.82	90.20	109.10	83.89	89	111	92	119
Ghali at al.	25	SM1.0	0.4	0.36	0.32	104.32	114.97	130.40	114.98	123	111	98	111
Ghali at al.	26	SM1.5	0.4	0.25	0.23	118.57	187.93	206.22	152.10	112	71	64	87
Luo and Durani	31	I.I	0.4	0.59	0.39	59.83	40.30	60.78	60.50	66	98	65	65
Luo and Durani	32	INT1	0.4	0.42	0.40	46.26	44.08	46.14	33.25	85	89	85	118
Luo and Durani	33	INT2	0.4	0.38	0.40	40.97	42.63	40.87	26.79	77	74	77	118
Islam and Park	34	1	0.4	0.39	0.31	29.64	30.68	38.57	30.49	103	99	79	100
Islam and Park	35	2	0.4	0.40	0.31	32.77	33.12	42.64	32.66	115	114	89	116
Islam and Park	36	3C	0.4	0.39	0.31	31.30	31.98	40.73	31.65	88.9	112	1.07	113
Hawkins et al.	37	S1	0.4	0.31	0.29	95.28	122.85	132.51	108.40	152	118	109	133
Hawkins et al.	38	S2	0.4	0.35	0.36	69.72	78.76	77.95	70.65	126	112	113	124
Hawkins et al.	39	S3	0.4	0.43	0.41	72.16	66.98	70.71	57.50	74	80	76	93
Hawkins et al.	40	S4	0.4	0.27	0.29	82.37	120.81	114.56	94.72	152	104	109	132
AVERAGE (%)										98	100	81	102
STANDART DEVIATION (%)										28	15	17	18

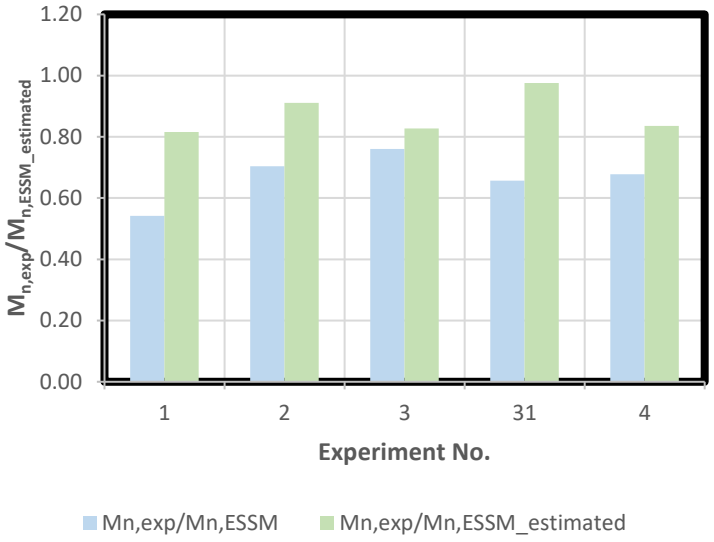

Figure 3.83 Moment Capacity Ratios, $M_{n,exp}/M_{n,ESSM}$ and $M_{n,exp}/M_{n,ESSM\_estimated}$ (For $V_u/V_n \leq 0.1$)

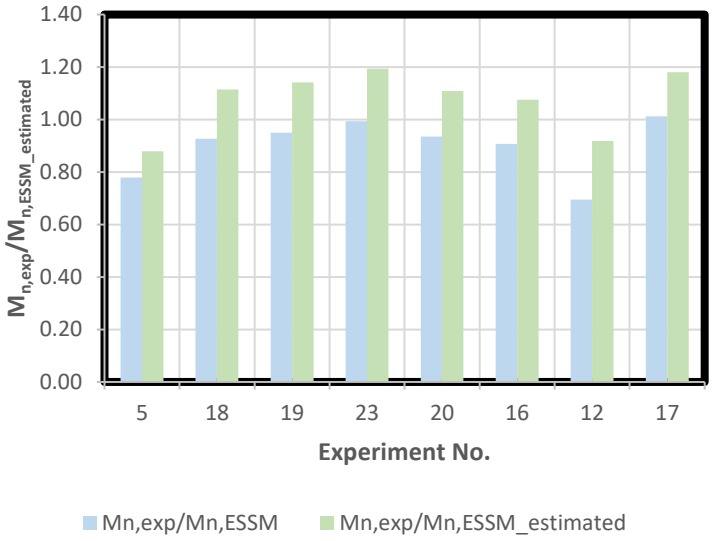

Figure 3.84 Moment Capacity Ratios, $M_{n,exp}/M_{n,ESSM}$ and $M_{n,exp}/M_{n,ESSM\_estimated}$ (For $0.1 < V_u/V_n \leq 0.2$)

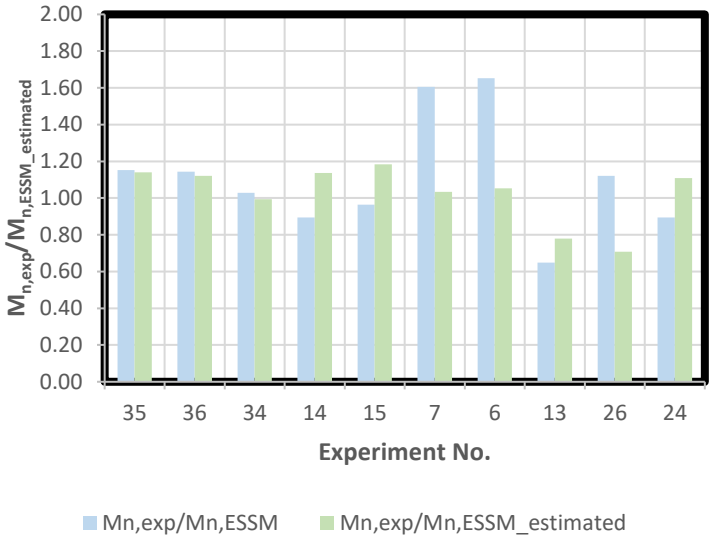

Figure 3.85 Moment Capacity Ratios, $M_{n,exp}/M_{n,ESSM}$ and $M_{n,exp}/M_{n,ESSM\_estimated}$ (For $0.2<V_u/V_n\leq0.3$)

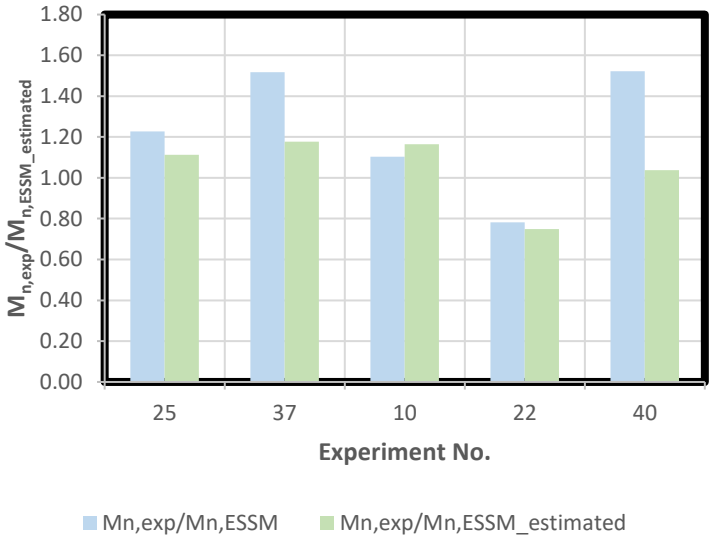

Figure 3.86 Moment Capacity Ratios, $M_{n,exp}/M_{n,ESSM}$ and $M_{n,exp}/M_{n,ESSM\_estimated}$ (For 0.3<Vu/Vn≤0.4)

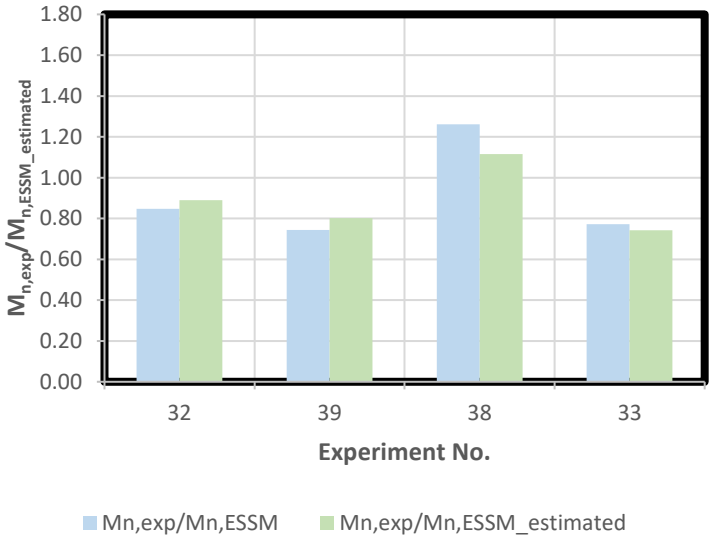

Figure 3.87 Moment Capacity Ratios, $M_{n,exp}/M_{n,ESSM}$ and $M_{n,exp}/M_{n,ESSM\_estimated}$ (For $0.4<Vu/Vn\leq0.5$)

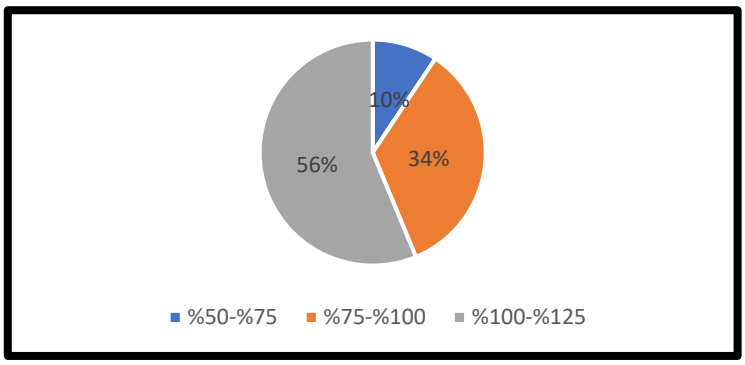

Figure 3.88 Distribution of $M_{n,exp}/M_{n,ESSM\_estimated}$ Results

3.5 Validation of Improved Model Using Different Dataset

In Section 3.4, eccentric shear stress model improved by deriving new formula for contribution factor, γ_v. In Section 3.5, different eccentric shear stress model approaches were compared and improved eccentric shear stress model was validated by using different dataset which is shown in Table 3.13. All specimens which are shown in Table 3.13 were tested by Muttoni and Beyer at 2016. All structural

member sizes are similar for every test specimen. In addition, effective depth of slab and compressive strength of concrete are very close to each other, therefore effects of these properties on strength of the slab column connections could be ignored. Flexural reinforcement ratio is approximately 0.8% and gravity shear ratio fluctuated between 0.24 and 0.8. All necessary parameters and test results are shown in Table 3.13.

Table 3.13 Parameters of Test Specimens and Results of Experiments (Muttoni and Beyer, 2016)

Researcher	Specimen	$L_1 \times L_2$, mm	$c_1 \times c_2$ mm	h, mm	d, mm	f_c, MPa	ρ, %	$V_{u,exp}$, kN	$M_{n,exp}$, kN.m
Muttoni and Beyer	PD1	3000×3000	390×390	250	204	37.9	0.79	253	525
Muttoni and Beyer	PD2	3000×3000	390×390	250	198	36.9	0.81	734	196
Muttoni and Beyer	PD3	3000×3000	390×390	250	198	34.9	0.81	734	200
Muttoni and Beyer	PD4	3000×3000	390×390	250	201	39	0.8	376	527
Muttoni and Beyer	PD5	3000×3000	390×390	250	198	37.5	0.81	517	462
Muttoni and Beyer	PD6	3000×3000	390×390	250	199	38.3	0.81	517	372
Muttoni and Beyer	PD8	3000×3000	390×390	250	198	32.7	0.81	376	384

Moment capacities of 7 test specimen were predicted with eccentric shear model approaches evaluated in Section 3.4 and results are shown in Table 3.14. As it is seen in Table 3.14, improved model gives good prediction compared to the other eccentric shear stress model approaches. However, it is clearly seen that improved model tends to overestimate moment capacity of the connection with high gravity shear ratio. The main reason is that test specimens used to derive γ_v equation varies approximately between 0%-48% in terms of gravity shear ratio. Gravity shear ratio is limited with 0.4 in ACI, and higher gravity shear ratios is not allowed to use in design process. Therefore, test specimens (PD2 and PD3) which have higher gravity shear ratio is extracted, mean and standard deviation of results were calculated again. Mean values of moment capacities are 153%, 139% and 135% for original eccentric shear stress model, eccentric shear stress model in Eurocode and improved eccentric shear stress

model, respectively. In addition, standard deviations are 21%, 24% and %15 for original eccentric shear stress model, eccentric shear stress model in Eurocode and improved eccentric shear stress model respectively. It is obvious that improved model predicts moment capacity of the slab column connections better compared to the ACI and Eurocode approaches. However, it is clearly seen that using of improved model for high gravity shear ratios is not proper. Therefore, gravity shear ratio should be limited with 0.4 and flexural reinforcement ratio should also be limited with 1.5% to use improved model. Otherwise, unexpected and unconservative results can be obtained.

Table 3.14 Predicted Moment Capacities of Test Specimens (Muttoni and Beyer, 2016)

Researcher	Specimen	V_u/V_n	$M_{n,ESSM}$(kN.m)	$M_{n,ESSM,estimated}$ (kN.m)	$M_{n,ESSM}$(kN.m) (Luo and Durani)	$M_{n,eurocode}$(kN.m)	$M_{n,exp}/M_{n,ESSM}$ (%)	$M_{n,exp}/M_{n,ESSM,estimated}$ (%)	$M_{n,exp}/M_{n,ESSM}$(%) (Luo and Durani)	$M_{n,exp}/M_{n,eurocode}$ (%)
Muttoni and Beyer	PD1	0.24	403.3	357.1	450.9	465.2	130	147	116	113
Muttoni and Beyer	PD2	0.74	129.1	291.3	145.7	102.8	152	67	134	191
Muttoni and Beyer	PD3	0.76	115.3	278.2	130.3	91.9	173	72	154	218
Muttoni and Beyer	PD4	0.36	335.8	349.3	377.3	372.3	157	151	140	142
Muttoni and Beyer	PD5	0.52	242.4	325.6	273.8	253.4	191	142	169	182
Muttoni and Beyer	PD6	0.51	251.7	332.7	284.2	263.4	148	112	131	141
Muttoni and Beyer	PD8	0.40	280.2	311.6	316.4	322.5	137	123	121	119
AVERAGE (%)							155	116	138	158
STANDART DEVIATION (%)							19	32	17	36

CHAPTER 4

CONCLUSIONS

Two punching design methods included in Turkish Specification, TBDY 2018, for flat plate slab-column connections were evaluated in this study. These methods are eccentric shear stress model and finite element-based design. In the scope of finite element-based design, two different approaches were examined. In the first approach, it is assumed that punching design is done according to maximum shear stress on the critical punching perimeter line at the critical side. In the second approach, punching design is done according to average shear stress on the critical punching perimeter line at the critical side. Moreover, effect of mesh size on the analysis results were studied. At the final stage of this study, the ratio of transferred moment carried by shear, $\gamma_{v,}$ estimated based on flexural reinforcement ratio and gravity shear ratio. Findings and results were presented below.

- After analysis of 30 test specimen, it is clearly seen that eccentric shear stress model estimates moment capacity of the slab-column connection well on average but with a high standard deviation. This means that if test specimens were evaluated individually, eccentric shear stress model can overestimate or underestimates the moment capacity of the connection. Especially, moment capacity of test specimens which have flexural reinforcement ratio on the slab smaller than %1 overestimated by using the eccentric shear stress model. If it is considered that slabs generally have flexural reinforcement ratio smaller than %1, eccentric shear stress model gives probably unsafe results.
- Design of connections using finite element model stress results with approach 1 is found very conservative. If approach 1 is used in design

process, shear stress is found to be very high compared to the actual stress for same loading conditions. Therefore, engineers probably should use shear reinforcement or strength enhancement methods based on the finite element model results. Optimum design for slab-column connection is not provided, and cost of the design increase by using finite element based-design method with approach 1.

- Approach 2 predicts moment capacity of the connection better compared to the approach 1. It still predicts moment capacity of the connection conservatively with mean value of moment capacity ratio, $M_{n,exp}/M_{n,FEM2}$ equal to %114. Unconservative results were obtained for some test specimens. Main reason of that is critical shear stress on the critical punching perimeter line is specified averagely for whole perimeter. However, finite element model results and actual results are not very different. So, it can be said that approach 2 estimates moment capacity of the connection close with actual moment capacity of the connection. Even if standard deviation is also high, it gives almost always gives conservative results compared to eccentric shear stress model. (See Figure 3.69)
- Eccentric shear stress model and finite element-based design were compared for biaxial lateral load condition. Results show that approach 1 (maximum shear stress-based design) is conservative compared to eccentric shear stress model. However, approach 2 (average shear stress-based design) gives similar results with eccentric shear stress model.
- Using of finer mesh (changing of mesh size from d/2 to d/4) for slab member in finite element models cause to estimate moment capacity of the connection high by increasing %9 for approach 2. Moreover, mean value of moment capacity ratio, $M_{n,exp}/M_{n,FEM2}$ decreases and come closer to %100. However, here important thing is that mesh size was arranged being higher than minimum aggregate size. In addition, mesh convergence study shows that results are converged with mesh size d/4.

- The proposed improved eccentric shear stress model estimates moment capacity of the connection better than other methods with low standard deviation. Number of test specimen is not enough for at the moment. Moreover, improvement was done only for test specimens which have square columns. Therefore, rectangular columns should be also considered, and number of test specimens which have rectangular column should be increased. However, improved model is good examples to represent effects of flexural reinforcement and gravity shear ratio on contribution of transferred moment carried by shear or flexure.

  Improved model gives unsafe results for some test specimens even if it predicts moment capacity of the connections close. These results were obtained for unfactored material properties and loads. During the design process, they are also predicted conservatively by using safety factors. That is why new γ_v equation is found from mean of results.
- It is observed that the ratio of transferred moment carried by shear, γ_v is affected from flexural reinforcement ratio and gravity shear ratio. The ratios of transferred moment carried by shear, $\gamma_{v,exp}$ which was calculated depending on the experimental results show that original eccentric shear stress model underestimates γ_v for flexural reinforcement ratio smaller than 1% and gravity shear ratio smaller than 0.3. Naturally, original eccentric shear stress model overestimates γ_v for flexural reinforcement ratio higher than 1% and gravity shear ratio higher than 0.3. (See Figures 3.77 and 3.78)

REFERENCES

ACI-Committee 318. (2019). Building Code Requirements for Concrete and Commentary. *ACI 318-19M*, 628. *American Concrete Institute*.

Binici, B., (2003) Punching Shear Strengthening of Reinforced Concrete Slabs Using Fiber Reinforced Polymers. *PhD Thesis, Department of Civil Engineering, University of Texas at Austin.*

CEB/fib Task Group. (2001). Punching of Structural Concrete Slabs. *International Federation of Structural Concrete.*

Choi, K. K., Shin, D. W., & Park, H. G. (2014). Modification of the ACI 318 design method for slab-column connections subjected to unbalanced moment. *Advances in Structural Engineering*, *17*(10), 1469–1480. https://doi.org/10.1260/1369-4332.17.10.1469

Durrani, A. J., Du, Y., & Luo, Y. H. (1995). Seismic resistance of nonductile slab-column connections in existing flat-slab buildings. *ACI Materials Journal*, *92*(4), 479–487. https://doi.org/10.14359/997

Farhey, D. N., Adin, M. A., & Yankelevsky, D. Z. (1993). RC Flat Slab-Column Subassemblages under Lateral Loading. *Journal of Structural Engineering*, *119*(6), 1903–1916. https://doi.org/10.1061/(asce)0733-9445(1993)119:6(1903)

Ghali, A., Elmasri, M. Z., & Dilger, W. (1976). Punching of Flat Plates Under Static and Dynamic Horizontal Forces. *J Am Concr Inst*, *73*(10), 566–572. https://doi.org/10.14359/11097

Hanson, N. W., & Hanson, J. M. (1968). Portland Cement Association Research and Development Laboratories Shear and Moment Transfer Between Concrete

Slabs and Columns. *Journal of the PCA Research and Development Laboratories*, *10*(1), 2–16.

Institution, T. S. (2018). Turkish Building Earthquake Code. *Ministry of Industry and Technology*, 416. http://www.resmigazete.gov.tr/eskiler/2018/03/20180318M1.pdf

Luo, Y. H., & Durrani, A. J. (1995). Equivalent beam model for flat-slab buildings - part I: interior connections. *ACI Structural Journal*, *92*(1), 115–124.

Megally, S., & Ghali, A. (2000). Punching shear design of earthquake-resistant slab-column connections. *ACI Structural Journal*, *97*(5), 720–730. https://doi.org/10.14359/8807

Morrison, D.G and Sozen, M.A. (1981). Response of Reinforced Concrete Plate-Column Connections to Dynamic and Static Horizontal Loads. *Civil Engineering Studies, Structural Research Series, No. 490, University of Illinois, Urbana, USA.*

Pan, A. D., & Moehle, J. P. (1992). An Experimental Study of Slab-Column Connections. *ACI Structural Journal, 89*, 626–638.

Park, H., & Choi, K. (2006). Improved Strength Model for Interior Flat Plate–Column Connections Subject to Unbalanced Moment. *Journal of Structural Engineering*, *132*(5), 694–704. https://doi.org/10.1061/(asce)0733-9445(2006)132:5(694)

Robertson, I. N., & Durrani, A. J. (1990). Seismic Response of Connections in Intermediate Flat-Slab Subassemblies. *Structural research at rice*, 41, 266.

Zhou, Y., & Hueste, M. B. D. (2017). Review of Test Data for Interior Slab-Column Connections with Moment Transfer. *ACI-fib International Symposium Punching shear of structural concrete slabs*, SP-315, 141-166

Zorlu, M. (2012). Evaluation of Punching Shear Strength Design and Modelling Approaches for Slab-Column Connections. *Master Thesis, Department of Civil Engineering, Middle East Technical University*

Drakatos, I. S., Muttoni, A., & Beyer, K. (2016). Internal slab-column connections under monotonic and cyclic imposed rotations. *Engineering Structures*, *123*, 501–516. https://doi.org/10.1016/j.engstruct.2016.05.038